

Robust transformation of singlet order into heteronuclear magnetisation over an extended coupling range

Christian Bengs, Laurynas Dagys, Malcolm H. Levitt

PII: S1090-7807(20)30168-3  
DOI: <https://doi.org/10.1016/j.jmr.2020.106850>  
Reference: YJMRE 106850

To appear in: *Journal of Magnetic Resonance*

Received Date: 21 August 2020  
Accepted Date: 9 October 2020

Please cite this article as: C. Bengs, L. Dagys, M.H. Levitt, Robust transformation of singlet order into heteronuclear magnetisation over an extended coupling range, *Journal of Magnetic Resonance* (2020), doi: <https://doi.org/10.1016/j.jmr.2020.106850>

This is a PDF file of an article that has undergone enhancements after acceptance, such as the addition of a cover page and metadata, and formatting for readability, but it is not yet the definitive version of record. This version will undergo additional copyediting, typesetting and review before it is published in its final form, but we are providing this version to give early visibility of the article. Please note that, during the production process, errors may be discovered which could affect the content, and all legal disclaimers that apply to the journal pertain.



# Robust transformation of singlet order into heteronuclear magnetisation over an extended coupling range

Christian Bengs<sup>a,\*</sup>, Laurynas Dagys<sup>a</sup> and Malcolm H. Levitt<sup>a</sup>

<sup>a</sup>*School of Chemistry, Southampton University, University Road, SO17 1BJ, UK*

## ARTICLE INFO

### Keywords:

Pulse sequence  
Singlet states  
Polarization transfer  
PHIP

## ABSTRACT

Several important NMR procedures involve the conversion of nuclear singlet order into heteronuclear magnetisation, including some experiments involving long-lived spin states and parahydrogen-induced hyperpolarization. However most existing sequences suffer from a limited range of validity or a lack of robustness against experimental imperfections. We present a new radio-frequency scheme for the transformation of the singlet order of a chemically-equivalent homonuclear spin pair into the magnetisation of a heteronuclear coupling partner. The proposed radio-frequency (RF) scheme is called gS2hM (generalized singlet-to-heteronuclear magnetization) and has good compensation for common experimental errors such as RF and static field inhomogeneities. The sequence retains its robustness for homonuclear spin pairs in the intermediate coupling regime, characterised by the in-pair coupling being of the same order of magnitude as the difference between the out-of-pair couplings. This is a substantial improvement to the validity range of existing sequences. Analytical solutions for the pulse sequence parameters are provided. Experimental results are shown for two test cases.

## 1. Introduction

Nuclear magnetic resonance (NMR) techniques are often limited by low polarisation levels and the restricted lifetime of nuclear spin order. These limitations put strong restrictions on many powerful NMR techniques such as correlation spectroscopy, diagnostic imaging, diffusion imaging and kinetic analysis [1–6]. Some of these issues may be circumvented by utilising nuclear long-lived spin states and hyperpolarization techniques. Nuclear long-lived spin states are spin ensemble configurations with exceptionally long relaxation lifetimes, often exceeding longitudinal relaxation time constants  $T_1$  by large factors [7–9]. Hyperpolarization techniques generate strong perturbations of the thermal equilibrium population distribution of the spin ensemble, leading, in favourable cases, to NMR signals enhanced by many orders of magnitude [10–15]. Long-lived states may be combined with hyperpolarization techniques in order to generate strongly enhanced spin order that persists for a relatively long time [16–26].

The seminal example of a nuclear long-lived spin state is the nuclear singlet order (SO) of coupled spin-1/2 pairs of the same isotopic type [9, 27–29]. Nuclear singlet order indicates a population imbalance between the nuclear singlet and triplet states. Although singlet order is not associated with observable magnetization, several techniques have been developed for converting observable magnetization into singlet order, and back again [30–40]. These techniques include the M2S (magnetization-to-singlet) and S2M (singlet-to-magnetization) pulse sequences [32, 33]. As originally designed, the M2S/S2M sequences operate best for spin systems in the near-equivalence regime, meaning that the members of the spin pair display a much stronger mutual coupling than the difference between their chemically-shifted resonance frequencies [41, 42]. Recent improvements have extended the operational range of the M2S/S2M sequences, leading to the generalized M2S (gM2S) and general-coupling M2S (gcM2S) methods [38–40]. The gcM2S method has been used for the spectral editing of complex biomolecular NMR spectra [39].

It is also possible to convert singlet order of a spin pair into magnetization of a third spin, which is of a different isotopic type [43]. Several different pulse sequences have been developed for this task, especially in the context of parahydrogen induced polarisation (PHIP) [35, 36, 44–51]. Although most such methods involve “two-channel” irradiation, i.e. the application of radiofrequency pulses at the resonance frequencies of both species, the requisite transformation may be achieved in a robust fashion by single-channel irradiation at the resonance frequency of the target spin alone [36, 50, 52–56]. The relevant pulse sequence is called S2hM (singlet-to-heteronuclear magnetization) [50, 57] and is closely

\*Corresponding author

cb2r15@soton.ac.uk (C. Bengs); l.dagys@soton.ac.uk (L. Dagys); mhl@soton.ac.uk (M.H. Levitt)  
www.chem.soton.ac.uk (C. Bengs)

## Generalised S2hM sequence

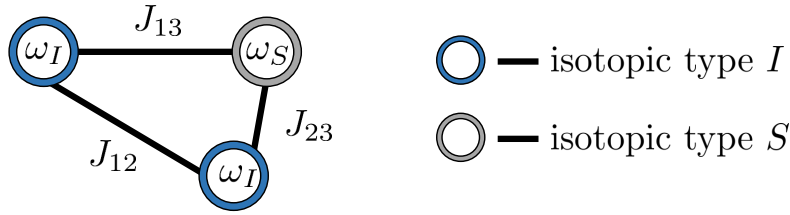


**Figure 1:** Schematic diagram of a AA'X system. The homonuclear spins  $I$  shown in blue are chemically equivalent but magnetically inequivalent. They have identical resonance frequencies, but differing coupling constants to the heteronuclear spin  $S$  shown in grey. The coupling regime depends on the angle  $\theta_{ST}$ , defined by equation 1.

related, but not identical, to the homonuclear S2M sequence [32, 33]. Like the S2M sequence, from which it is derived, the S2hM sequence is best adapted to the near-equivalence regime.

To facilitate the discussion, consider a AA'X system of the type shown in figure 1. The homonuclear spins are assumed to be of the same isotopic type  $I$ , such as  $^1\text{H}$  for example, whereas the out-of-pair partner belongs to a different isotopic type  $S$ , such as  $^{13}\text{C}$ . The  $I$ -spins are assumed to have identical resonance frequencies  $\omega_I/2\pi$ , which is satisfied for chemically equivalent spins, or for chemically inequivalent spin pairs in low magnetic field [58–62]. The members of the homonuclear spin pair have different couplings ( $J_{13} \neq J_{23}$ ) to the out-of-pair partner. The difference in the heteronuclear couplings induces singlet-triplet mixing of the  $I$ -spin pair. The coupling regime of the homonuclear pair may be characterised by a singlet-triplet mixing angle  $\theta_{ST}$ , defined as follows:

$$\theta_{ST} = \tan^{-1}((J_{13} - J_{23})/2J_{12}), \quad (1)$$

where  $J_{12}$  represents the homonuclear coupling, and  $J_{13}$ ,  $J_{23}$  describe the out-of-pair couplings to the heteronucleus. A mixing angle of  $\theta_{ST} = 0$  corresponds to exact magnetic equivalence. The near-equivalence regime corresponds to small values of  $\theta_{ST}$ . A mixing angle of  $\theta_{ST} \sim \pi/4$  indicates the intermediate coupling regime, while a mixing angle of  $\theta_{ST} \simeq \pi/2$  represents the case of strong inequivalence, often known as “weak coupling” [41, 42].

The amplitude for the transformation of homonuclear singlet order into heteronuclear magnetization is denoted here by the symbol  $\zeta$ . An explicit definition of  $\zeta$  is given below. It has a maximum achievable value of  $\zeta = 1$ . The operational regime of a pulse sequence is conveniently represented by plotting numerical evaluations of  $\zeta$  against the mixing angle  $\theta_{ST}$ .

Plots of  $\zeta$  against  $\theta_{ST}$  are shown for three different pulse sequences in figure 2. One of the first pulse sequences proposed for this task was designed by Goldman and Jóhannesson [46]. Its performance is shown by the black line in figure 2(a). As seen in the plot, the Goldman-Jóhannesson sequence performs well for the intermediate-coupling regime, but its performance declines sharply in both the near-equivalence and strong inequivalence regimes. The performance of the S2hM sequence [50, 57] is shown by the blue curve. For small mixing angles  $\theta_{ST}$  (the near-equivalence regime), the S2hM sequence is able to efficiently transform singlet polarisation into heteronuclear Zeeman polarisation with an amplitude close to the theoretical maximum. However, the performance of S2hM rapidly declines at larger mixing angles.

The pulse sequence described in the current paper is called gS2hM (generalized S2hM). Its performance is shown by the orange line in figure 2(a). For small mixing angles  $\theta_{ST}$ , the S2hM and gS2hM sequences both transform singlet order into heteronuclear Zeeman polarisation with efficiencies close to the theoretical maximum. However, the operational regime of the gS2hM sequence is considerably wider than that of S2hM, covering a range of mixing angles spanning  $0^\circ < \theta_{ST} \lesssim 50^\circ$ , albeit with prominent dips in performance at certain  $\theta_{ST}$  values. However, as discussed below, these dips may be flattened out by modifying the echo numbers.

When comparing pulse sequences, it is also important to take into account their robustness with respect to common experimental imperfections. Figure 2(b) compares the performance of the three pulse sequences again, but this time in the presence of a distribution of static magnetic fields. A normal distribution of resonance offsets is simulated, with standard deviation equal to twice the characteristic frequency  $\omega_e = 2\pi\{J_{12}^2 + \frac{1}{4}(J_{13} - J_{23})^2\}^{1/2}$ . This quantity

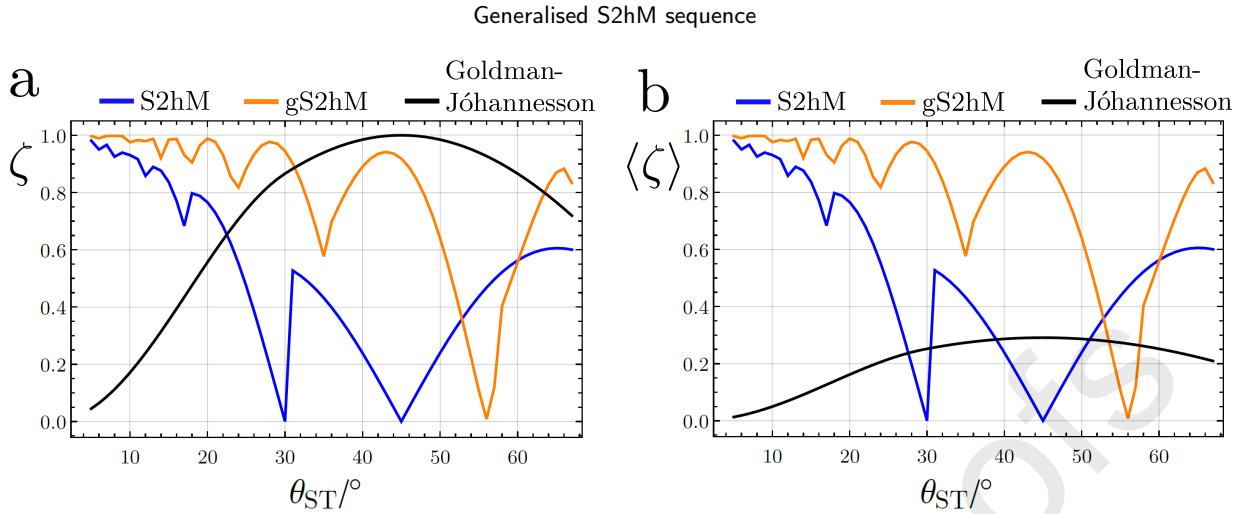


**Figure 2:** Numerical simulations of the transformation amplitude  $\zeta$  for  $I$ -spin singlet order into  $S$ -spin Zeeman polarisation (equation 9), plotted as a function of singlet-triplet mixing angle  $\theta_{ST}$ . Small mixing angles represent the near-equivalent regime, whereas large mixing angles represent strong inequivalence. The intermediate regime corresponds roughly to  $20^\circ \lesssim \theta_{ST} \lesssim 60^\circ$ . Blue lines: Numerical simulations of the single-channel S2hM sequence, using pulse sequence parameters given by the analytic solutions given in reference 50. Black lines: Numerical simulations of the single-channel Goldman-Jóhannesson sequence [46], using pulse sequence parameters given by the analytic solutions in reference 63. Orange lines: Numerical simulations of the single-channel gS2hM sequence, using pulse sequence parameters given by the analytic solutions in table 1. In all cases, relaxation is neglected and radio-frequency pulses are assumed to have a negligible duration. (a) Transformation amplitudes for a perfectly homogeneous static magnetic field distribution. (b) Transformation amplitudes averaged over an inhomogeneous static magnetic field distribution. Static magnetic field variations have been sampled according to a normal distribution of resonance offsets with standard deviation equal to twice the characteristic frequency  $\omega_e = 2\pi\{J_{12}^2 + \frac{1}{4}(J_{13} - J_{23})^2\}^{1/2}$ .

represents the magnitude of the relevant part of the spin Hamiltonian, independent of the angle  $\theta_{ST}$ , which varies across the plot. As may be seen in figure 2(b), the performance of the S2hM and gS2hM sequences is almost unchanged, while the performance of the Goldman-Jóhannesson sequence is strongly degraded. The response of the different pulse sequences to experimental imperfections is discussed in more detail below.

The rest of this paper presents the theory and construction principles of gS2hM. Experimental results are shown which illustrate the performance of gS2hM in realistic contexts. A more thorough comparison of gS2hM with other pulse sequences, especially those used in the context of *para*-hydrogen induced polarization, is given in the discussion section.

## 2. Theory

The following theory was developed with the assistance of *SpinDynamica* software [64].

### 2.1. Transformation Amplitude

Consider a three-spin-1/2 system with spins (1, 2) being of isotopic type  $I$  and spin (3) being of isotopic type  $S$ . The state of the spin ensemble is described by a density operator  $\rho$ . Following reference [50], the degree of  $I$ -spin singlet order in the spin ensemble is denoted  $p_S^I$ , and is given by:

$$p_S^I = \langle \rho \rightarrow P_S^I \rangle \quad (2)$$

where the symbol  $\langle A \rightarrow B \rangle$  is called the *operator amplitude* of  $B$  in  $A$ , and is defined as follows:

$$\langle A \rightarrow B \rangle := \text{Tr} \{ AB \} / \text{Tr} \{ BB^\dagger \}. \quad (3)$$

The singlet polarisation level operator  $P_S^I$  is given by [50]

$$P_S^I = -\frac{1}{2} \mathbf{I}_1 \cdot \mathbf{I}_2 \quad (4)$$

Similarly, the degree of  $S$ -spin Zeeman polarization is denoted  $p_z^S$ , and is given by:

$$p_z^S = \langle \rho \rightarrow P_z^S \rangle \quad (5)$$

where the Zeeman polarisation level operator [50] is defined as follows:

$$P_z^S = \frac{1}{4} S_{3z}. \quad (6)$$

The singlet order  $p_S^I$  and Zeeman polarisation  $p_z^S$  are bounded, as shown below:

$$\begin{aligned} -\frac{1}{3} &\leq p_S^I \leq +1 \\ -1 &\leq p_z^S \leq +1, \end{aligned} \quad (7)$$

The transformation amplitude of operator  $A$  into operator  $B$  by a unitary transformation  $V$  is defined by

$$\langle A \xrightarrow{V} B \rangle := \text{Tr} \{ A V B V^\dagger \} / \text{Tr} \{ B B^\dagger \}. \quad (8)$$

The transformation amplitude under  $V$  is constrained by the eigenvalue spectra of the two operators  $A$  and  $B$ . The corresponding bounds are known as the *unitary constraints* for the transformation of  $A$  into  $B$  [65, 66].

Our main interest is the transformation amplitude of  $I$ -spin singlet order into  $S$  spin Zeeman polarisation

$$\zeta = \langle P_S^I \xrightarrow{V} P_z^S \rangle, \quad (9)$$

which is bounded by  $-1 \leq \zeta \leq 1$  [66]. This indicates that any amount of singlet order  $p_S^I$  may in principle be fully converted into  $S$ -spin Zeeman polarisation  $p_z^S$  by coherent evolution under a pulse sequence.

## 2.2. Hamiltonian reduction

Our primary interest lies in AA'X spin systems characterised by the following rotating-frame Hamiltonian [42]

$$H_0 = \Omega_I^0 (I_{1z} + I_{2z}) + \Omega_S^0 S_{3z} + 2\pi J_{12} \mathbf{I}_1 \cdot \mathbf{I}_2 + 2\pi J_{13} I_{1z} S_{3z} + 2\pi J_{23} I_{2z} S_{3z}. \quad (10)$$

The AA' spins are of isotopic type  $I$  and the X spin is of isotopic type  $S$ . The resonance frequency of the two  $I$ -spins is assumed to be identical so that both  $I$ -spins display identical resonance offset behaviour described by a single resonance offset frequency  $\Omega_I^0 = \omega_I^0 - \omega_{\text{ref}}$  given in  $\text{rad s}^{-1}$ . Similarly,  $\Omega_S^0 = \omega_S^0 - \omega_{\text{ref}}$  represents the resonance offset frequency of spin  $S$  in  $\text{rad s}^{-1}$ . The scalar coupling constants in Hz are denoted by  $J_{ij}$ . The Hamiltonian  $H_0$  may be decomposed as follows

$$\begin{aligned} H_0 &= H_A + H_B, \\ H_A &= \omega_{II} \mathbf{I}_1 \cdot \mathbf{I}_2 + \frac{1}{2} \omega_{IS}^\Delta (I_{1z} - I_{2z}) S_{3z}, \\ H_B &= \Omega_I^0 (I_{1z} + I_{2z}) + \Omega_S^0 S_{3z} + \frac{1}{2} \omega_{IS}^\Sigma (I_{1z} + I_{2z}) S_{3z}. \end{aligned} \quad (11)$$

Here,  $\omega_{II}^\Delta = 2\pi J_{12}$  denotes the homonuclear coupling,  $\omega_{IS}^\Delta = 2\pi(J_{13} - J_{23})$  denotes the difference between the out-of-pair and  $\omega_{IS}^\Sigma = 2\pi(J_{13} + J_{23})$  the sum of the out-of-pair scalar couplings (all in  $\text{rad s}^{-1}$ ). The terms  $H_A$  and  $H_B$  commute

$$[H_A, H_B] = 0, \quad (12)$$

which may be used to show that the Hamiltonian  $H_B$  takes no active role in the manipulation of singlet order. We will therefore focus on the Hamiltonian  $H_A$ .

The Hamiltonian  $H_A$  may be separated into two independent parts acting on the  $\alpha$  and  $\beta$  subspace of the  $S$  spin, respectively

$$\begin{aligned} H_A &= H_A^\alpha + H_A^\beta, \\ H_A^\alpha &= \left( \omega_{II} \mathbf{I}_1 \cdot \mathbf{I}_2 + \frac{1}{4} \omega_{IS}^\Delta (I_{1z} - I_{2z}) \right) S^\alpha, \\ H_A^\beta &= \left( \omega_{II} \mathbf{I}_1 \cdot \mathbf{I}_2 - \frac{1}{4} \omega_{IS}^\Delta (I_{1z} - I_{2z}) \right) S^\beta. \end{aligned} \quad (13)$$

The operators  $S^\alpha$  and  $S^\beta$  are the corresponding projectors onto the  $\alpha$  and  $\beta$  subspace of spin  $S$  [41]

$$S^\alpha = \frac{1}{2} \mathbb{1} + S_{3z}, \quad S^\beta = \frac{1}{2} \mathbb{1} - S_{3z}. \quad (14)$$

A slight shift of notation reinforces the algebraic similarities between the Hamiltonian of an AA'X system and an AA' spin system

$$\begin{aligned} H_A^\alpha &= \left( \omega_{II} \mathbf{I}_1 \cdot \mathbf{I}_2 + \frac{1}{2} \Omega_\Delta (I_{1z} - I_{2z}) \right) S^\alpha, \\ H_A^\beta &= \left( \omega_{II} \mathbf{I}_1 \cdot \mathbf{I}_2 - \frac{1}{2} \Omega_\Delta (I_{1z} - I_{2z}) \right) S^\beta, \end{aligned} \quad (15)$$

where we have defined  $\Omega_\Delta = \frac{1}{2} \omega_{IS}^\Delta$ .

The terms  $H_A^\alpha$  and  $H_A^\beta$  are identical to the Hamiltonians of a coupled spin-1/2 pair with  $\Omega_\Delta$  taking the role of the (rotating-frame) resonance offset frequency [40, 42]. Motivated by this observation we introduce the singlet-triplet mixing angle  $\theta_{ST}$  and an effective angular frequency  $\omega_e$ :

$$\theta_{ST} = \tan^{-1} \left( \frac{\Omega_\Delta}{\omega_{II}} \right) = \tan^{-1} \left( \frac{\omega_{IS}^\Delta}{2\omega_{II}} \right), \quad (16)$$

$$\omega_e = \sqrt{\omega_J^2 + \Omega_\Delta^2} = \sqrt{(\omega_{II})^2 + \frac{1}{4}(\omega_{IS}^\Delta)^2}. \quad (17)$$

The mixing angle is defined in such a way that magnetically equivalent  $I$ -spins display a mixing angle  $\theta_{ST} = 0$  and strongly inequivalent  $I$ -spins display a mixing angle  $\theta_{ST} \simeq \pi/2$ . The Hamiltonians  $H_A^\alpha$  and  $H_A^\beta$  take the form

$$\begin{aligned} H_A^\alpha &= \omega_e \left( \cos(\theta_{ST}) \mathbf{I}_1 \cdot \mathbf{I}_2 + \frac{1}{2} \sin(\theta_{ST}) (I_{1z} - I_{2z}) \right) S^\alpha, \\ H_A^\beta &= \omega_e \left( \cos(\theta_{ST}) \mathbf{I}_1 \cdot \mathbf{I}_2 - \frac{1}{2} \sin(\theta_{ST}) (I_{1z} - I_{2z}) \right) S^\beta. \end{aligned} \quad (18)$$

### 2.3. Singlet-triplet evolution

Further analysis is conveniently carried out by a convenient choice of basis. Consider first a basis formed by nuclear singlet-triplet states for spin  $I$  and a basis formed by the conventional Zeeman states for spin  $S$

$$\begin{aligned} \mathcal{B}_S &= \{ |\alpha\rangle, |\beta\rangle \}, \\ \mathcal{B}_I &= \{ |S_0\rangle, |T_{+1}\rangle, |T_0\rangle, |T_{-1}\rangle \}, \end{aligned} \quad (19)$$

with the nuclear singlet and triplet states being defined as follows

$$\begin{aligned} |S_0\rangle &= (|\alpha\beta\rangle - |\beta\alpha\rangle)/\sqrt{2}, & |T_{+1}\rangle &= |\alpha\alpha\rangle, \\ |T_0\rangle &= (|\alpha\beta\rangle + |\beta\alpha\rangle)/\sqrt{2}, & |T_{-1}\rangle &= |\beta\beta\rangle. \end{aligned} \quad (20)$$

The basis states of  $\mathcal{B}_I$  and  $\mathcal{B}_S$  are used to construct the following basis states

$$\begin{aligned}\tilde{\mathcal{B}}_S &= \left\{ \frac{1}{\sqrt{2}}(|\alpha\rangle + |\beta\rangle), \frac{1}{\sqrt{2}}(|\alpha\rangle - |\beta\rangle) \right\} := \left\{ |n_1^S\rangle, |n_2^S\rangle \right\}, \\ \tilde{\mathcal{B}}_I &= \left\{ |S_0\rangle, |T_0\rangle, \frac{1}{\sqrt{2}}(|T_+\rangle + |T_-\rangle), \frac{1}{\sqrt{2}}(|T_+\rangle - |T_-\rangle) \right\} := \left\{ |n_1^I\rangle, |n_2^I\rangle, |n_3^I\rangle, |n_4^I\rangle \right\}.\end{aligned}\quad (21)$$

For the remainder of this section we work with the following direct product basis derived from the states  $\tilde{\mathcal{B}}_S$  and  $\tilde{\mathcal{B}}_I$

$$\begin{aligned}\mathcal{B} &= \left\{ |1\rangle = |n_2^I n_2^S\rangle, |2\rangle = |n_1^I n_1^S\rangle, |3\rangle = |n_3^I n_2^S\rangle, |4\rangle = |n_4^I n_2^S\rangle, \right. \\ &\quad \left. |5\rangle = |n_2^I n_1^S\rangle, |6\rangle = |n_1^I n_2^S\rangle, |7\rangle = |n_3^I n_1^S\rangle, |8\rangle = |n_4^I n_1^S\rangle \right\},\end{aligned}\quad (22)$$

For example the state  $|1\rangle = |n_2^I n_2^S\rangle$  is given by

$$\begin{aligned}|1\rangle &= |n_2^I n_2^S\rangle = |T_0\rangle \otimes \frac{1}{\sqrt{2}}(|\alpha\rangle - |\beta\rangle) \\ &= \frac{1}{\sqrt{2}}(|T_0\alpha\rangle - |T_0\beta\rangle) = \frac{1}{2}(|\alpha\beta\alpha\rangle + |\beta\alpha\alpha\rangle - |\alpha\beta\beta\rangle - |\beta\alpha\beta\rangle).\end{aligned}\quad (23)$$

It proves convenient to add a multiple of the unity operator to the Hamiltonian  $H_A$ :

$$H_A \rightarrow H_A + \frac{\omega_{II}}{4} \mathbb{1}.\quad (24)$$

This is possible since the unity operator commutes with all other operators and its presence in the Hamiltonian has no effect on the spin dynamics.

This allows the terms  $H_A^\alpha$  and  $H_A^\beta$  to be expressed as follows:

$$\begin{aligned}\tilde{H}_A^\alpha &= H_A^\alpha + \frac{\omega_{II}}{4} \mathbb{1} = \omega_e \left( \sin(\theta_{ST}) I_x^{12} + \cos(\theta_{ST}) I_z^{12} + \frac{1}{2} \cos(\theta_{ST}) \mathbb{1}^{34} \right), \\ \tilde{H}_A^\beta &= H_A^\beta + \frac{\omega_{II}}{4} \mathbb{1} = \omega_e \left( \sin(\theta_{ST}) I_x^{56} + \cos(\theta_{ST}) I_z^{56} + \frac{1}{2} \cos(\theta_{ST}) \mathbb{1}^{78} \right),\end{aligned}\quad (25)$$

with  $I_\mu^{rs}$  being a single-transition operator along the Cartesian axis  $\mu$  and  $\mathbb{1}^{rs}$  the identity on  $\{r, s\}$  [67, 68].

For both  $\tilde{H}_A^\alpha$  and  $\tilde{H}_A^\beta$  the non-trivial part induces transitions between the  $|S_0\rangle$  and  $|T_0\rangle$  states of the  $I$  spins, whereas the identity part causes pure phase evolution. Within the single-transition operator formalism [67, 68], the free evolution propagator  $U_0(\tau)$  is given by

$$U_0(\tau) = U_0^{12}(\tau) U_0^{34}(\tau) U_0^{56}(\tau) U_0^{78}(\tau)\quad (26)$$

where the individual propagators are

$$\begin{aligned}U_0^{12}(\tau) &= R^{12}(\tfrac{1}{2}\omega_e\tau, \theta_{ST}), & U_0^{34}(\tau) &= \Phi^{34}(\tfrac{1}{2}\omega_e\cos\theta_{ST}\tau), \\ U_0^{56}(\tau) &= R^{56}(\tfrac{1}{2}\omega_e\tau, \theta_{ST}), & U_0^{78}(\tau) &= \Phi^{78}(\tfrac{1}{2}\omega_e\cos\theta_{ST}\tau).\end{aligned}\quad (27)$$

The operator  $R^{ij}(\alpha, \beta)$  represents a sequence of rotations around the  $(y, z, y)$  axes, while  $\Phi^{rs}(\gamma)$  generates pure phase evolution through the angle  $\gamma$ :

$$\begin{aligned}R^{ij}(\alpha, \beta) &= R_y^{ij}(-\beta) R_z^{ij}(\alpha) R_y^{ij}(\beta) \\ \Phi^{rs}(\gamma) &= \exp \{-i\gamma \mathbb{1}^{rs}\}.\end{aligned}\quad (28)$$

## Generalised S2hM sequence

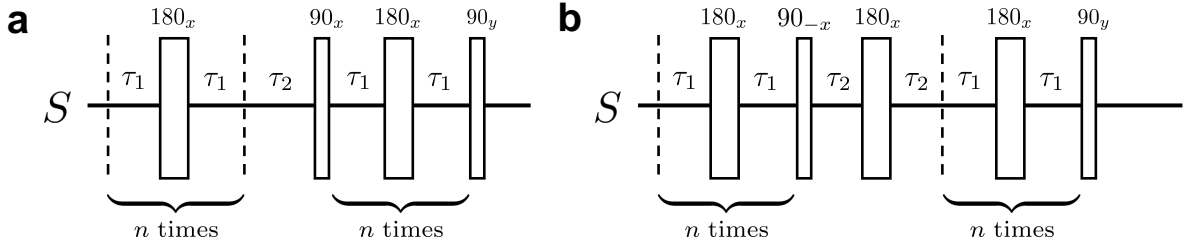


**Figure 3:** **a)** Singlet-to-heteronuclear-Magnetisation (S2hM) pulse sequence. **b)** generalised Singlet-to-heteronuclear-Magnetisation (gS2hM) pulse sequence. The final 90° pulses are included in both the S2hM and gS2hM sequences, so that  $I$ -spin singlet order is transformed into  $S$ -spin Zeeman order. Both sequences only involve radiofrequency irradiation on the  $S$ -spin channel.

## 2.4. Heteronuclear spin echoes

A detailed overview of the S2hM and gS2hM sequence are given in figure 3. Both sequences make heavy use of spin echo blocks of the type  $\{\tau - \pi_x^S - \tau\}$ , where the  $\pi$ -pulse is solely applied to the  $S$ -spins. The propagator for a single echo event may be simplified by expressing the  $S$ -spin  $x$ -pulse generator in terms of single transition operators generated by the basis states of equation 22

$$S_{3x} = -I_z^{12} - \frac{1}{2} \mathbb{1}^{34} + I_z^{56} + \frac{1}{2} \mathbb{1}^{78}. \quad (29)$$

The operator for a rotation of the  $S$ -spin through an angle  $\beta$  around the  $x$ -axis may be written as follows:

$$R_x^S(\beta) = \exp\{-i\beta S_{3x}\} = R_z^{12}(-\beta)\Phi^{34}(-\beta/2)R_z^{56}(\beta)\Phi^{78}(\beta/2). \quad (30)$$

This may be combined with the free evolution propagator of equation 26 to give the following form for the  $S$ -spin echo propagator:

$$U_{SE}(\tau) = U_0(\tau) - R_x^S(\pi) - U_0(\tau) = U_{SE}^{12}(\tau)U_{SE}^{34}(\tau)U_{SE}^{56}(\tau)U_{SE}^{78}(\tau). \quad (31)$$

The effective echo propagators  $U_{SE}^{ij}$  may be shown to induce fictitious rotations within their respective subspaces [40]

$$\begin{aligned} U_{SE}^{12}(\tau) &= R^{12}(\xi, \psi), & U_{SE}^{34}(\tau) &= \Phi^{34}(-\pi/2 + \omega_e \cos \theta_{ST} \tau), \\ U_{SE}^{56}(\tau) &= R^{56}(\xi, \psi)\Phi^{56}(-\pi), & U_{SE}^{78}(\tau) &= \Phi^{78}(\pi/2 + \omega_e \cos \theta_{ST} \tau), \end{aligned} \quad (32)$$

with angles  $\psi$  and  $\xi$  given by

$$\begin{aligned} \psi &= \cot^{-1} \left( \csc(2\theta_{ST}) (\cot^2(\frac{1}{2}\omega_e \tau) - \cos(2\theta_{ST})) \right), \\ \xi &= -2 \cos^{-1} \left( \cos(\theta_{ST}) \sin(\omega_e \tau) \right). \end{aligned} \quad (33)$$

For simplicity we suppress the explicit time-dependence of  $\xi(\tau)$  and  $\psi(\tau)$ .

A physical interpretation of the angles  $\xi$  and  $\psi$  is as follows: The angle  $\psi$  represents a tilt angle defining the orientation of the effective rotation axis in the  $xz$ -plane, with  $\psi = 0$  corresponding to rotation around the  $z$ -axis. The angle  $\xi$  represents the net rotation angle of the echo propagator.

## 2.5. The S2hM sequence

Extensive descriptions of the S2hM sequence may be found in references 50 and 57. Here we briefly highlight some key aspects illustrating the limitations of the S2hM approach. As shown in figure 3a, the S2hM sequence converts homonuclear singlet order into heteronuclear magnetisation by two sets of heteronuclear spin echoes synchronised with the effective angular frequency of the system, bracketing an additional delay and a central  $\pi/2$  pulse [50, 57]. The S2hM echo delay  $\tau_1$ , and the phase evolution delay  $\tau_2$ , are given by

$$\tau_1 = \tau_2 = \pi/(2\omega_e). \quad (34)$$

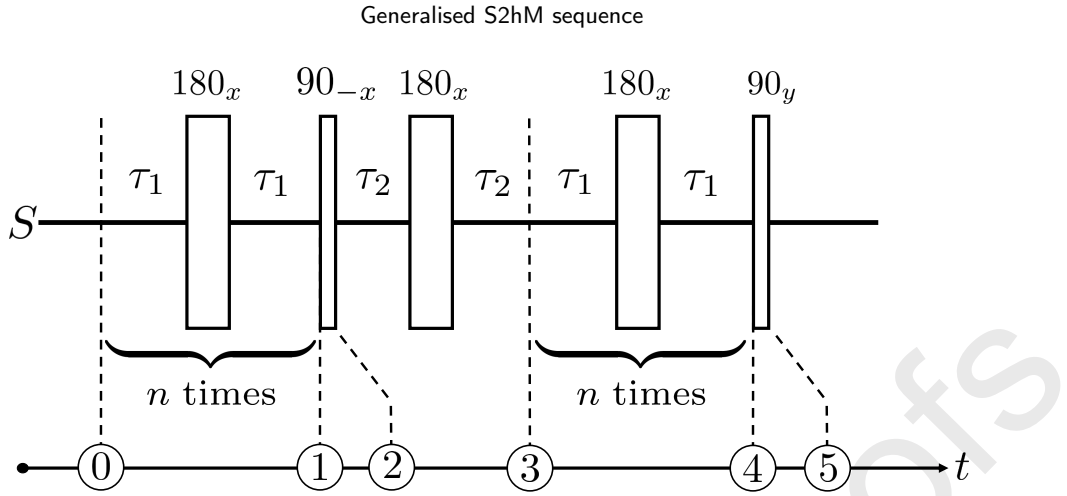


**Figure 4:** The generalised Singlet-to-heteronuclear-Magnetisation (gS2hM) pulse sequence. Note that there are no pulses on the  $I$ -spin channel. The indicated time points are referenced in the text.

The loop number of the S2hM sequence depends on the mixing angle  $\theta_{ST}$  as follows:

$$n_{S2hM} = \text{round}(\pi/(4\theta_{ST})). \quad (35)$$

As discussed in reference 57, the derivation of equations 34 and 35 relies on small mixing angles  $\theta_{ST} \ll 1$ , corresponding to the near-equivalence regime. Under this assumption the tilt angle  $\psi$  of the  $S$  spin echo propagator is given approximately by

$$\psi(\tau_1) = \psi(\pi/(2\omega_e)) \simeq \pi/2 \quad (\theta_{ST} \ll 1). \quad (36)$$

The desired tilt angle of  $\psi = \pi/2$  may be generated even outside the regime of small  $\theta_{ST}$  by setting the echo evolution delay  $\tau_1$  as follows:

$$\tau_1 = 2\omega_e^{-1} \cot^{-1}(\sqrt{\cos(2\theta_{ST})}), \quad (37)$$

which reduces to  $\tau_1 = \pi/(2\omega_e)$  as  $\theta_{ST}$  tends towards zero. However, this equation does not admit any physical solutions for mixing angles  $\theta_{ST} \geq \pi/4$ . The S2hM sequence is therefore fundamentally limited to spin systems with mixing angles  $\theta_{ST} < \pi/4$ . Figure 2 indicates that the performance of S2hM rapidly decreases as a function of  $\theta_{ST}$ , well before the fundamental limit of  $\theta_{ST} = \pi/4$ .

Although the S2hM sequence converts  $I$ -spin singlet order into  $S$ -spin magnetization, the resulting magnetization is not distributed evenly amongst the  $S$ -spin transitions. Indeed, as shown in references 50 and 57, the  $S$ -spin magnetization is concentrated on the inner transitions of the  $S$ -spin multiplet. The density operator transformation achieved by the S2hM pulse sequence may therefore be written:

$$U_{S2hM} P_S^I U_{S2hM}^\dagger \simeq P_{z,IT}^S + \text{orthogonal operators} \quad (38)$$

where “IT” stands for “inner transitions”. The operator for the selective z-polarization of the inner transitions of the  $S$ -spin multiplet is given by:

$$P_{z,IT}^S = P_z^S (\mathbb{1} - I_{1z} I_{2z}) \quad (39)$$

The selective transfer of  $I$ -spin singlet order into the central peak of the  $S$ -spin multiplet is prominently visible in, for example, figure 1d of reference 50.

**Table 1**

Key quantities, optimal evolution delays, and echo numbers for the gS2hM sequence.

$\theta_{ST}$	$\tan^{-1}(J_{\Delta}/2J_{12})$	$n^*$	$\text{round}(\pi/\xi^*)$
$\omega_e$	$2\pi\sqrt{J_{12}^2 + J_{\Delta}^2}/4$	$\tau_1^*$	$\cos^{-1}(2 - J_{\Delta}/2J_{12} - 4J_{\Delta}/(2J_{12} + J_{\Delta}))$
$\xi^*$	$2 \sec^{-1} \left( (2J_{12} + J_{\Delta}) / \sqrt{4J_{12}^2 + 4J_{12}J_{\Delta} - J_{\Delta}^2} \right)$	$\tau_2^*$	$2\omega_e^{-1} \cot^{-1} \sqrt{\left( 12J_{12}^2 + \sqrt{128J_{12}^4 + J_{\Delta}^4} \right) / (4J_{12}^2 + J_{\Delta}^2)}$

## 2.6. The gS2hM sequence

The S2hM sequence accomplishes the transformation in equation 38 with high efficiency for small values of  $\theta_{ST}$ . The gS2hM sequence accomplishes the same transformation over a wider range of  $\theta_{ST}$  values.

Consider the detailed breakdown of the gS2hM sequence in figure 4. The spin density operators at the indicated time points are denoted  $\rho_0, \rho_1 \dots \rho_5$ . The operation of the pulse sequence may be explained by expressing the density operators at the different time points in terms of single-transition operators [68, 69], using the basis states given in equation 22. Assume an *initial* state of pure *I*-spin singlet order. The density operator  $\rho_0$  may be written as follows:

$$\rho_0 = P_S^I = -\frac{1}{2}(I_z^{12} + I_z^{56}) - \frac{1}{4}(\mathbb{1}^{34} + \mathbb{1}^{78}) + \frac{1}{8}\mathbb{1}, \quad (40)$$

Assume that the *final* state  $\rho_5$  is given approximately by the operator  $P_{x,IT}^S$ , as defined in equation 39. This implies that the *penultimate* state before the final *S*-spin  $\pi/2$  pulse should be given by

$$\rho_4 \simeq P_{x,IT}^S \quad (41)$$

where the operator for selective *x*-magnetization on the inner *S*-spin transitions is given by

$$P_{x,IT}^S = P_x^S (\mathbb{1} - I_{1z}I_{2z}) \quad (42)$$

This operator may be written in terms of single-transition operators as follows:

$$P_{x,IT}^S = -\frac{1}{2}(I_z^{12} - I_z^{56}) - \frac{1}{4}(\mathbb{1}^{34} + \mathbb{1}^{78}) + \frac{1}{8}\mathbb{1} \quad (43)$$

By comparing equations 40 and 43, it may be seen that the desired transformation of *I*-spin singlet order into inner-transition *S*-spin magnetization is accomplished by a pulse sequence whose propagator leads to the following transformations:

1. The operator  $I_z^{56}$  should be inverted in sign;
2. The operator  $I_z^{12}$  should be preserved without sign change;
3. The states  $\{|3\rangle, |4\rangle, |7\rangle, |8\rangle\}$  may each accumulate an arbitrary phase shift, but should not mix with other states.

Equations 26 and 30 show that intervals of free evolution, and *S*-spin pulses with phase 0, both induce selective rotations in the  $\{|1\rangle, |2\rangle\}$  and  $\{|5\rangle, |6\rangle\}$  subspaces, and hence fulfil the last of the three conditions above. An appropriate pulse sequence may therefore be constructed from a sequence of evolution intervals and *S*-spin *x*-pulses which invert the sign of the *z*-operator for the  $\{|5\rangle, |6\rangle\}$  subspace, at the same time as preserving the sign of the *z*-operator for the  $\{|1\rangle, |2\rangle\}$  subspace. The problem of pulse sequence design reduces to finding the combination of *S*-spin *x*-pulses and evolution delays which implement these two simultaneous operator transformations, for as wide a range of  $\theta_{ST}$  values as possible.

The gS2hM sequence accomplishes these transformations in four steps, which may be summarized as follows:

$$\begin{array}{ccccccccc}
 I_z^{12} & \xrightarrow{\text{step 1}} & -I_x^{12} & \xrightarrow{\text{step 2}} & -I_y^{12} & \xrightarrow{\text{step 3}} & -I_x^{12} & \xrightarrow{\text{step 4}} & I_z^{12} \\
 I_z^{56} & \longrightarrow & -I_x^{56} & \longrightarrow & I_y^{56} & \longrightarrow & I_x^{56} & \longrightarrow & -I_z^{56} \\
 (0) & & (1) & & (2) & & (3) & & (4)
 \end{array} \quad (44)$$

where the bracketed numbers refer to the time points in figure 4.

The individual steps in equation 44 are implemented as follows.

- *Step 1.* This is implemented by applying a series of  $n$  heteronuclear spin echoes of the form  $\{\tau_1 - \pi_x^S - \tau_1\}$  whose effective rotation axis has a tilt angle of  $\psi = \pi/4$ , instead of the tilt angle of  $\psi = \pi/4$  used in the S2hM sequence. A similar approach was used in the design of the gM2S sequence [40].

The tilt angle of  $\psi = \pi/4$  is imposed by choosing the echo delay such that  $\tau_1 = \tau_1^*$ , where  $\tau_1^*$  is defined as follows:

$$\tau_1^* := 2\omega_e^{-1} \tan^{-1}(1/\sqrt{\cos(2\theta_{ST})}). \quad (45)$$

The effective frequency  $\omega_e$  is given by equation 17. For this particular choice of echo delay  $\tau_1$ , the tilt angle  $\psi$  is given by  $\psi = \pi/4$ , and the effective rotation angle  $\xi$  of the spin echo element is equal to

$$\xi^* := \xi(\tau_1^*) = 2 \sec^{-1} \left( \frac{\cos(\theta_{ST}) + \sin(\theta_{ST})}{\sqrt{\cos(2\theta_{ST}) + \sin(2\theta_{ST})}} \right). \quad (46)$$

According to equation 31, the overall propagator of a single echo block  $\{\tau_1^* - \pi_x^S - \tau_1^*\}$  is given by

$$U_{SE}(\tau_1^*) = \{R^{12}(\xi^*, \pi/4)\Phi^{34}(-\pi/2 + \omega_e \cos \theta_{ST} \tau_1^*)\} \times \{R^{56}(\xi^*, \pi/4)\Phi^{56}(-\pi)\Phi^{78}(\pi/2 + \omega_e \cos \theta_{ST} \tau_1^*)\}. \quad (47)$$

Such echo blocks may be constructed for mixing angles  $0 < \theta_{ST} \leq 67.5^\circ$ . A series of  $n$  consecutive spin echoes of the form  $\tau_1^* - \pi_x^S - \tau_1^*$  has the following propagator:

$$[U_{SE}(\tau_1^*)]^n = \{R^{12}(n\xi^*, \pi/4)\Phi^{34}(-n\pi/2 + n\omega_e \cos \theta_{ST} \tau_1^*)\} \times \{R^{56}(n\xi^*, \pi/4)\Phi^{56}(-n\pi)\Phi^{78}(n\pi/2 + n\omega_e \cos \theta_{ST} \tau_1^*)\}. \quad (48)$$

Now assume that the echo number  $n$  satisfies the following condition:

$$n\xi^* = \pi, \quad (49)$$

Since  $n$  is an integer and  $\xi^*$  is real, this condition may only be satisfied exactly for certain values of  $\theta_{ST}$ . Hence, the following analysis is only approximate, in general. Assuming that equation 49 is satisfied exactly, the following argument shows that the rotation operators  $R^{ij}(n\xi^*, \pi/4)$  produce  $(\pi/2)_y$  rotations within their respective subspaces (within a phase factor):

$$R^{ij}(n\xi^*, \pi/4) = R^{ij}(\pi, \pi/4) = R_y^{ij}(\pi/4)R_z^{ij}(\pi)R_y^{ij}(-\pi/4) = R_y^{ij}(\pi/2)R_z^{ij}(\pi). \quad (50)$$

The overall propagator of the echo block may therefore be written as follows:

$$[U_{SE}(\tau_1^*)]^n = \{R_y^{12}(-\pi/2)R_z^{12}(-\pi)\}\{R_y^{56}(-\pi/2)R_z^{56}(-\pi)\Phi^{56}(-n\pi)\}W^{34}W^{78}, \quad (51)$$

with  $W^{34}$  and  $W^{78}$  generating unimportant phase evolution within subspaces  $\{|3\rangle, |4\rangle\}$  and  $\{|7\rangle, |8\rangle\}$ :

$$W^{ij} = \Phi^{ij}(n\pi/2 + n\omega_e \cos \theta_{ST} \tau_1^*). \quad (52)$$

The echo block propagator in equation 51 generates the desired transformations:

$$[U_{SE}(\tau_1^*)]^n I_z^{12} [U_{SE}(\tau_1^*)]^{n\dagger} = -I_x^{12} \quad (53)$$

$$[U_{SE}(\tau_1^*)]^n I_z^{56} [U_{SE}(\tau_1^*)]^{n\dagger} = -I_x^{56} \quad (54)$$

- *Step 2.* Equation 30 shows that the  $(90)_{-x}^S$  pulse induces z-rotations in the  $\{|1\rangle, |2\rangle\}$  and  $\{|5\rangle, |6\rangle\}$  subspaces through an angle  $\pi/2$  about the z-axes of the single-transition subspaces, but in opposite directions:

$$R_x^S(-\pi/2) I_x^{12} R_x^S(-\pi/2)^\dagger = R_z^{12}(\pi/2) I_x^{12} R_z^{12}(\pi/2)^\dagger = I_y^{12} \\ R_x^S(-\pi/2) I_x^{56} R_x^S(-\pi/2)^\dagger = R_z^{56}(-\pi/2) I_x^{56} R_z^{56}(-\pi/2)^\dagger = -I_y^{56} \quad (55)$$

This generates the crucial sign difference between the operators in the  $\{|1\rangle, |2\rangle\}$  and  $\{|5\rangle, |6\rangle\}$  subspaces.

## Generalised S2hM sequence

- *Step 3.* This step converts the single-transition  $y$ -operators into single-transition  $x$ -operators, without a sign change. This is accomplished, to a reasonable approximation, by a single spin echo of the form  $\tau_2 - \pi_x^S - \tau_2$ , with a suitable choice of the interval  $\tau_2$ .

According to equation 32, the spin density components  $I_y^{12}$  and  $I_y^{56}$  undergo identical evolution under the spin echo:

$$\begin{aligned} U_{SE}^{12}(\tau_2) I_y^{12} U_{SE}^{12}(-\tau_2) &= x(\tau_2) I_x^{12} + y(\tau_2) I_y^{12} + z(\tau_2) I_z^{12} \\ U_{SE}^{56}(\tau_2) I_y^{56} U_{SE}^{56}(-\tau_2) &= x(\tau_2) I_x^{56} + y(\tau_2) I_y^{56} + z(\tau_2) I_z^{56} \end{aligned} \quad (56)$$

with the following coefficients

$$\begin{aligned} x(\tau_2) &= 2 \cos(\theta_{ST}) \sin(\omega_e \tau_2) (\cos^2(\theta_{ST}) \cos(\omega_e \tau_2) + \sin^2(\theta_{ST})), \\ y(\tau_2) &= -\cos(\theta_{ST}) \cos(2\omega_e \tau_2) - \sin^2(\theta_{ST}), \\ z(\tau_2) &= 4 \cos^2(\theta_{ST}) \sin(\theta_{ST}) \sin^2(\frac{1}{2}\omega_e \tau_2) \sin(\omega_e \tau_2). \end{aligned} \quad (57)$$

The spin density operator components  $I_y^{12}$  and  $I_y^{56}$  are approximately aligned with the  $x$ -axis by choosing  $\tau_2$  so as to minimise the function

$$f(\tau_2) = y^2(\tau_2) + z^2(\tau_2). \quad (58)$$

The function  $f(\tau_2)$  is minimized at  $\tau_2 = \tau_2^*$ , where  $\tau_2^*$  is defined as follows:

$$\tau_2^* := 2\omega_e^{-1} \cot^{-1} \sqrt{3 \cos^2(\theta_{ST}) + \sqrt{8 \cos^4(\theta_{ST}) + \sin^4(\theta_{ST})}}. \quad (59)$$

Hence the required transformations of step 3 are approximately satisfied:

$$\begin{aligned} U_{SE}(\tau_2^*) I_y^{12} U_{SE}(\tau_2^*)^\dagger &\simeq I_x^{12} \\ U_{SE}(\tau_2^*) I_y^{56} U_{SE}(\tau_2^*)^\dagger &\simeq I_x^{56} \end{aligned} \quad (60)$$

- *Step 4.* Step 4 is achieved by applying the same spin echo block as used in Step 1. From the propagator in equation 51, this generates the following transformations:

$$[U_{SE}(\tau_1^*)]^n I_x^{12} [U_{SE}(\tau_1^*)]^{n\dagger} = -I_z^{12} \quad (61)$$

$$[U_{SE}(\tau_1^*)]^n I_x^{56} [U_{SE}(\tau_1^*)]^{n\dagger} = -I_z^{56} \quad (62)$$

The four steps may be chained together as in equation 44, giving the desired transformation property of the complete gS2hM sequence:

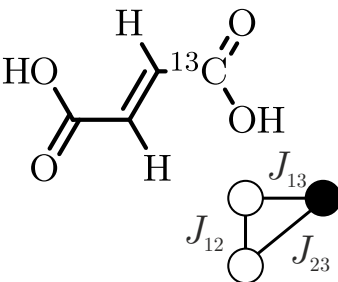
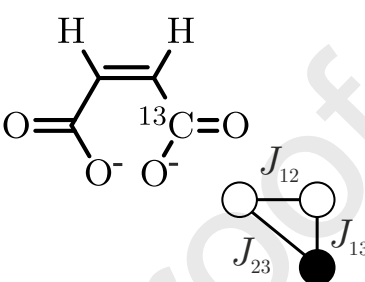
$$U_{gS2hM} P_S^I U_{gS2hM}^\dagger \simeq P_{z,IT}^S + \text{orthogonal operators} \quad (63)$$

Hence, the gS2hM sequence, with the parameter choices given in table 1, provides a reasonably accurate conversion of  $I$ -spin singlet order into  $x$ -magnetization of the  $S$ -spin inner transitions, over a wide range of  $\theta_{ST}$  values. The overall transformation is approximate since (i) equation 49 is satisfied exactly only at specific values of  $\theta_{ST}$ , and (ii) the function in equation 58 is not set to zero at  $\tau_2 = \tau_2^*$ , but only minimized.

The orange curve in figure 2(a) shows the performance of the gS2hM sequence as a function of  $\theta_{ST}$ , with the key quantities and timing parameters summarised in table 1. For the most part the transformation amplitudes  $\zeta$  for the gS2hM sequence are reasonably close to the theoretical maximum transformation amplitude of  $\zeta_{\max} = 1$  but display occasional dips in performance resulting in a saw-tooth profile. These dips are observed at  $\theta_{ST}$  values such that the quantity  $\pi/\xi^*$  is a half-integer, so that equation 49 is a particularly poor approximation. The most serious dips are at  $\theta_{ST} \simeq 35.42^\circ$  and  $\theta_{ST} \simeq 57.67^\circ$ . The latter dip is serious enough to limit the applicability of gS2hM to singlet-triplet mixing angles  $0 < \theta_{ST} \lesssim 50^\circ$ . In addition the transformation amplitude displays a monotonic decline as  $\theta_{ST}$  increases,

**Table 2**

Chemical structures of 1-<sup>13</sup>C-fumaric acid (*trans*-[1-<sup>13</sup>C]-but-2-endioic acid) and the 1-<sup>13</sup>C-maleate anion (*cis*-[1-<sup>13</sup>C]-but-2-endioate), which are the dominant species in the preparations used for the experiments. The relevant nuclei and their spin-spin couplings are indicated. The magnitude of the *J*-couplings were determined by fitting experimental data with numerical simulations (see sections 4.1 and 4.2). All couplings are assumed to be positive, as predicted by *Gaussian* calculations [70]. The M2S parameters for 1-<sup>13</sup>C-fumaric acid and 1-<sup>13</sup>C-maleate were optimised empirically.

fumaric acid		maleate	
			
$J_{12}/\text{Hz}$	$15.9 \pm 0.15$	$J_{12}/\text{Hz}$	$12.3 \pm 0.30$
$J_{13}/\text{Hz}$	$3.3 \pm 0.10$	$J_{13}/\text{Hz}$	$2.1 \pm 0.10$
$J_{23}/\text{Hz}$	$5.9 \pm 0.10$	$J_{23}/\text{Hz}$	$13.2 \pm 0.40$
$\theta_{\text{ST}}/^\circ$	$4.49 \pm 0.05$	$\theta_{\text{ST}}/^\circ$	$24.28 \pm 1.20$
$\tau_{\text{M2S}}/\text{ms}$	15.7	$\tau_{\text{M2S}}/\text{ms}$	21.3
$n_{\text{M2S}}$	7	$n_{\text{M2S}}$	1

which is associated with the finite value of the function  $f(\tau_2)$ , at the echo delay  $\tau_2 = \tau_2^*$  (equation 59). Despite these defects, the gS2hM sequence provides a reasonably accurate transformation of *I*-spin singlet order into heteronuclear magnetization over a much broader range of  $\theta_{\text{ST}}$  values than the S2hM sequence, including the important intermediate coupling regime. In addition, the gS2hM sequence is robust with respect to common instrumental imperfections, as discussed below.

An alternative method for choosing the echo numbers in the gS2hM sequence is given in Appendix 1. This approach stabilises the performance of the gS2hM sequence and smooths out the worst sawtooth dips. However this method involves a more complicated algorithm for choosing the echo numbers and leads in general to a longer pulse sequence duration. The “basic” parameter choices, as summarized in table 1, are assumed for the remainder of this article.

### 3. Experimental

#### 3.1. Samples

NMR experiments were performed on <sup>13</sup>C-labelled fumaric acid (*trans*-[1-<sup>13</sup>C]-but-2-endionate) and <sup>13</sup>C-labelled maleic acid (*cis*-[1-<sup>13</sup>C]-but-2-endionate), both purchased from Sigma-Aldrich.

A 8.3 mM 1-<sup>13</sup>C-fumaric acid solution was prepared by dissolving 0.5 mg of the substance in 0.5 ml of acetone-<sub>d</sub><sub>6</sub>, and transferring to a conventional 5 mm NMR tube. Under these conditions, the dissolved fumaric acid remains predominantly in the undissociated form, as shown by the structure in table 2 (left column). The *J*-coupling parameters were estimated by fitting simulations of the S2hM transfer to experimental data presented in the following sections, and are in good agreement with previously reported values [50, 57]. The signs of the coupling constants were determined by *Gaussian* calculations [70]. The singlet-triplet mixing angle of  $\theta_{\text{ST}} \approx 4.5^\circ$  places the <sup>1</sup>H spin pair of 1-<sup>13</sup>C-fumaric acid in the near-equivalence regime.

A 6.6 mM sample of 1-<sup>13</sup>C maleic acid was prepared by dissolving 0.54 mg of the substance in 0.7 ml of D<sub>2</sub>O, followed by transfer to a conventional 5 mm NMR tube. In aqueous solution, the labile protons of maleic acid are transferred to water forming maleate anions and hydronium cations. The structure of the 1-<sup>13</sup>C-maleate anion is shown in table 2 (right column), together with the scalar coupling parameters, which were estimated by fitting simulations of the S2hM transfer to experimental data presented in the following sections. The signs were determined by *Gaussian*

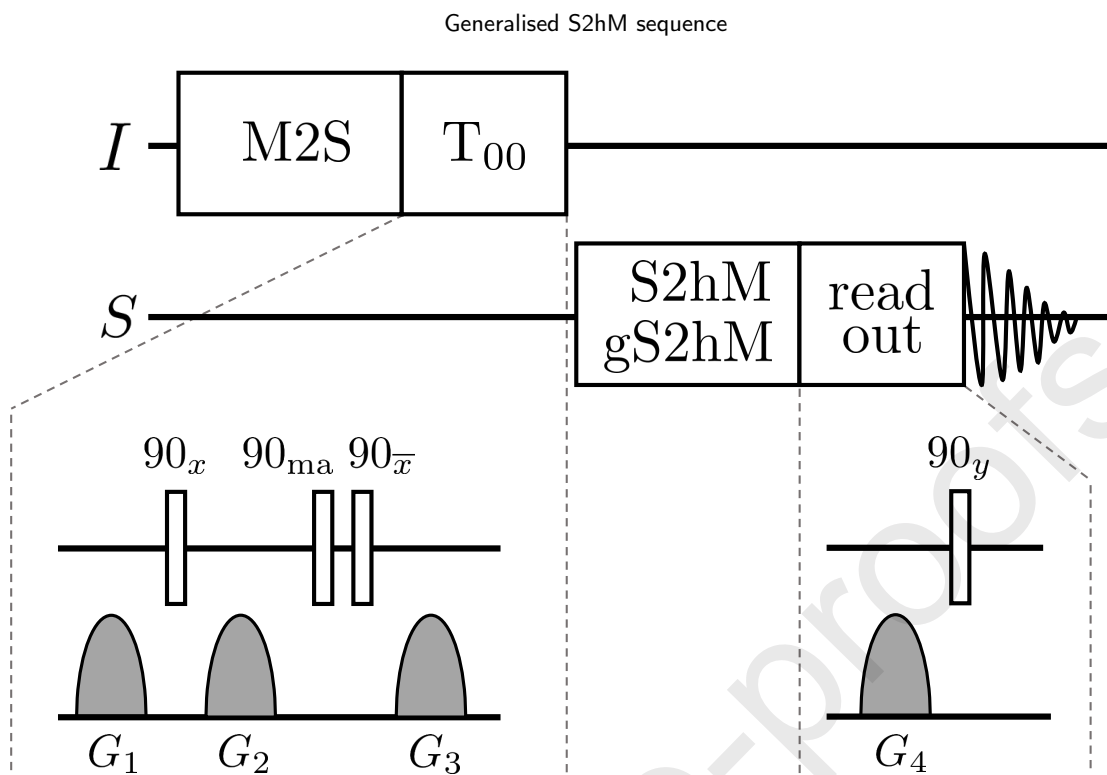


**Figure 5:** Pulse sequence protocol. Singlet order preparation on the  $I$  spin channel consists of a M2S block and a singlet order filtration element ( $T_{00}$ ). Singlet order is converted into heteronuclear magnetisation through application of an S2hM/gS2hM block on the  $S$  spin channel. The signal detection is initiated by application of a read out sequence. The singlet filter is given by a sequence of radio-frequency pulses and field gradient pulses. The phase angle "ma" indicates the magic angle  $\approx 54.7^\circ$  [71, 72]. The read-out sequence consists of a field gradient pulse for suppressing potential antiphase signal components followed by excitation of transverse magnetisation by a  $90_y$  pulse.

calculations [70]. The singlet-triplet mixing angle of  $\theta_{ST} \approx 24.28^\circ$  places the  $^1\text{H}$  spin pair of  $1\text{-}^{13}\text{C}$ -maleate in the intermediate coupling regime.

### 3.2. Instrumental

All experiments were carried out on a 400 MHz Bruker Avance Neo system. The recycling delays between transients were set to 20 s and 30 s for fumaric and maleic acid respectively. The pulse nutation frequencies were  $\sim 18.9$  kHz for  $^1\text{H}$  and  $\sim 22.3$  kHz for  $^{13}\text{C}$ . The data from  $1\text{-}^{13}\text{C}$ -fumaric acid was averaged over 2 transients with 131 k sampling points and a spectral width of 160 ppm. The data from  $1\text{-}^{13}\text{C}$ -maleic acid was averaged over 8 transients with 131 k sampling points and a spectral width of 160 ppm.

### 3.3. Pulse Sequences

An overview of the experimental protocol is given in figure 5. The pulse sequence steps operate as follows:

1. The initial M2S block excites homonuclear singlet order starting from a thermally polarised state. The M2S pulse sequence parameters for the two compounds are summarised in table 2. A formal description of the M2S sequence in  $\text{AA}'\text{X}$  systems may be found in reference 57.
2. The  $T_{00}$  block acts as a filter suppressing all NMR signals not passing through singlet order [71]. The field gradient parameters are summarised in table 3.
3. The S2hM or gS2hM block on the heteronuclear channel converts homonuclear singlet order into longitudinal heteronuclear magnetisation.

## Generalised S2hM sequence

**Table 3**

Field gradient and radiofrequency pulse specifications.

	<sup>1</sup> H channel	<sup>13</sup> C channel		
rf field nutation frequency	18.9 kHz	22.3 kHz		
	$T_{00}$ filter			read-out sequence
	$G_1$	$G_2$	$G_3$	$G_4$
gradient strength	15 G/cm	-8 G/cm	-7 G/cm	7.5 G/cm
duration	2.2 ms	1.0 ms	1.2 ms	4.0 ms

**Table 4**

Theoretical and experimental pulse sequence parameters for the solution of 1-<sup>13</sup>C-fumaric acid. The analytical optimum parameters  $n^*$ ,  $\tau_1^*$  and  $\tau_2^*$  were derived from the coupling values in table 2 using reference [50] for the S2hM sequence and table 1 for the gS2hM sequence. The experimentally optimized parameters are denoted  $n^{\text{exp}}$ ,  $\tau_1^{\text{exp}}$  and  $\tau_2^{\text{exp}}$ .

	S2hM	gS2hM
$n^* = n^{\text{exp}}$	10	15
$\tau_1^*/\text{ms}$	15.6	15.0
$\tau_1^{\text{exp}}/\text{ms}$	15.8	14.9
$\tau_2^*/\text{ms}$	15.6	7.9
$\tau_2^{\text{exp}}/\text{ms}$	15.8	8.1

- The read-out block on the heteronuclear channel consists of a field gradient pulse which suppresses unwanted single-quantum coherences, followed by excitation of transverse magnetization by a single  $\pi/2$  pulse, and acquisition of the NMR signal. The suppression of transverse magnetization before the final  $\pi/2$  pulse reduces the phase distortions of the resulting spectrum. The field gradient parameters are summarised in table 3.

All individual pulses for the M2S, S2hM and gS2hM sequences were replaced by their composite pulse counterparts, as follows:  $180_\phi$  pulses were replaced by  $90_{90+\phi}$   $180_\phi$   $90_{90+\phi}$  sequences;  $90_\phi$  pulses were replaced by  $180_{97.2+\phi}$   $360_{291.5+\phi}$   $180_{97.2+\phi}$   $90_\phi$  sequences [73, 74]. The free evolution delays were adjusted to account for the longer pulse element durations. For example, an echo delay was shortened by half the duration of the composite refocusing pulse element. The echo blocks for the S2hM and gS2hM sequences were additionally supercycled using a repeated (0,180°) phase scheme [75].

## 4. Results

### 4.1. 1-<sup>13</sup>C-Fumaric acid

The experimental procedure in figure 5 was applied to 1-<sup>13</sup>C-fumaric acid in order to study the relative performance of S2hM and gS2hM in a nearly-equivalent AA'X system. Figures 6(a,b) show the dependence of the <sup>13</sup>C signal amplitudes for 1-<sup>13</sup>C-fumaric acid on the echo delays  $\tau_1$  and  $\tau_2$ . Experimental results (orange) are complemented by *SpinDynamica* simulations (blue) [64]. Experimental data sets and simulations were both normalized by dividing the data by the maximum amplitude in the series. The  $\tau_1$ -dependence displays a rather complex behaviour without a straightforward interpretation. The oscillatory behaviour in Figure 6(b) represents the rotational motion of the spin density operator components  $I_x^{12}$  and  $I_x^{56}$  around their respective z-axes during step 2 of the gS2hM sequence. The good agreement between theory and experiment is gratifying.

Figures 6(a,b) indicate optimal gS2hM performance for  $\tau_1^{\text{exp}} = 14.9$  ms and  $\tau_2^{\text{exp}} = 8.1$  ms. These values agree well with theoretical predictions, as shown in table 4.

The dependence of <sup>13</sup>C signal amplitude on echo number  $n$  was also explored, fixing the echo delays  $\tau_1^{\text{exp}}$  and  $\tau_2^{\text{exp}}$  to their optimal values. The results shown in figure 6(c) indicate a slowly oscillating pattern. This is because the small

## Generalised S2hM sequence

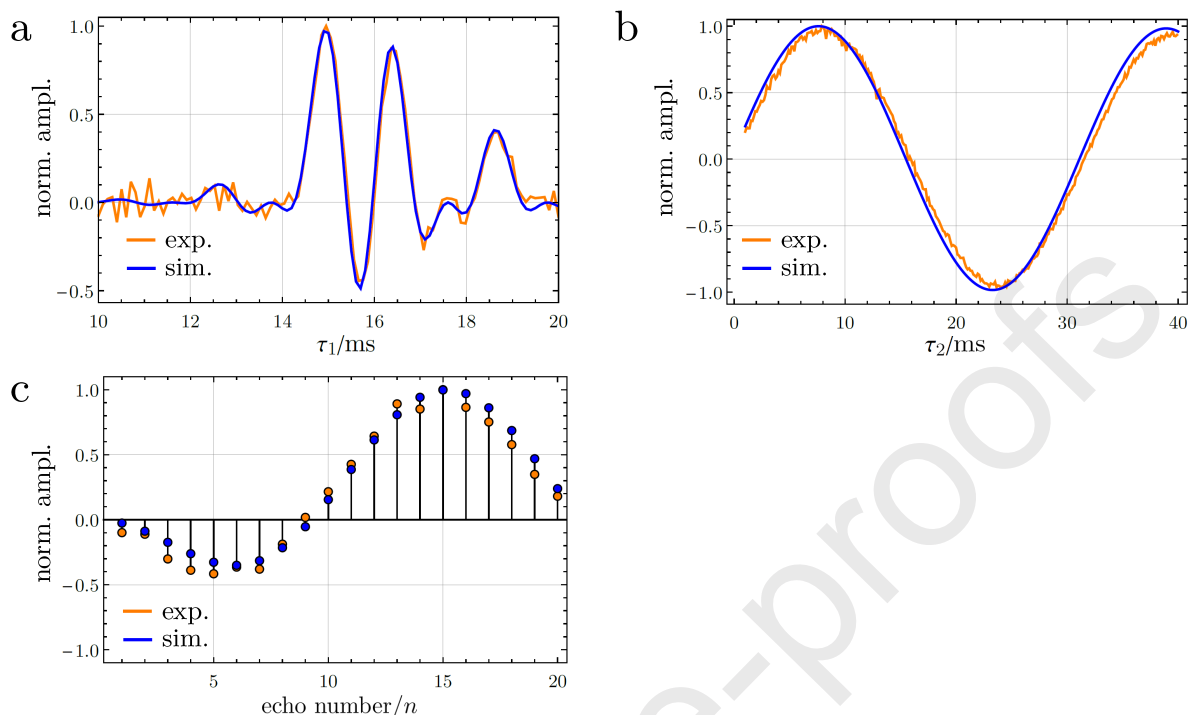


**Figure 6:** Experimental and simulated  $^{13}\text{C}$  signal amplitudes for 1- $^{13}\text{C}$ -fumaric acid solution. The experiments were performed according to the scheme in figure 5, varying the gS2hM parameters. Simulations were performed for the gS2hM transfer step assuming the coupling and pulse sequence parameters in tables 2 and 3. The experimental data sets (orange) and simulations (blue) were normalised to unity by dividing each data point by the maximum amplitude in the series. (a) Signal amplitude as a function of the echo interval  $\tau_1$  with fixed interval  $\tau_2 = 7.9$  ms and echo number  $n = 15$ . (b) Signal amplitude as a function of the free evolution delay  $\tau_2$  with fixed interval  $\tau_1 = 14.9$  ms and echo number  $n = 15$ . (c) Signal amplitude as a function of the echo number  $n$  with fixed intervals  $\tau_1 = 14.3$  ms and  $\tau_2 = 8.1$  ms.

value of  $\theta_{\text{ST}}$  for 1- $^{13}\text{C}$ -fumaric acid only allows the necessary spin order transformations to be built up in a cumulative fashion [33, 57].

Figure 7 shows  $^{13}\text{C}$  spectra of 1- $^{13}\text{C}$ -fumaric acid solution, obtained by the protocol in figure 5, using the M2S sequence to generate  $^1\text{H}$  singlet order, and either the S2hM or gS2hM sequences for the transformation of  $^1\text{H}$  singlet order into  $^{13}\text{C}$  magnetization. As expected, the performances of S2hM and gS2hM are very similar for this near-equivalent system. The central peak appears to be slightly less intense for the gS2hM spectrum, as compared to S2hM, but the outer peaks of the  $^{13}\text{C}$  multiplet are more prominent for gS2hM and more in phase with the central transition. The ratio of integrated spectral amplitudes is given by  $a_{\text{gS2hM}}/a_{\text{S2hM}} = 0.92$ .

The procedure given in Appendix 2 was used to obtain an experimental estimate of the transformation amplitude  $\zeta$  for the two sequences. This procedure is similar to that used to evaluate the S2hM sequence [50]. The estimates of the experimental transformation amplitudes are  $\zeta = 0.81 \pm 0.05$  for gS2hM and  $\zeta = 0.88 \pm 0.06$  for S2hM, in the case of 1- $^{13}\text{C}$ -fumaric acid solution. The small deviations from the theoretical values are attributed to relaxation losses and experimental imperfections.

#### 4.2. 1- $^{13}\text{C}$ -Maleic acid

The relative performance of the S2hM and gS2hM sequences for an intermediate-regime AA'X system was studied by applying the experimental protocol in figure 5 to the solution of 1- $^{13}\text{C}$ -maleic acid. The  $^{13}\text{C}$  signal amplitudes for 1- $^{13}\text{C}$ -maleic acid solution as a function of the echo delays  $\tau_1$  and  $\tau_2$  are displayed in figures 8(a,b). The experimental results (orange) are complemented by *SpinDynamica* simulations (blue) [64]. Experimental data sets and simulations

## Generalised S2hM sequence

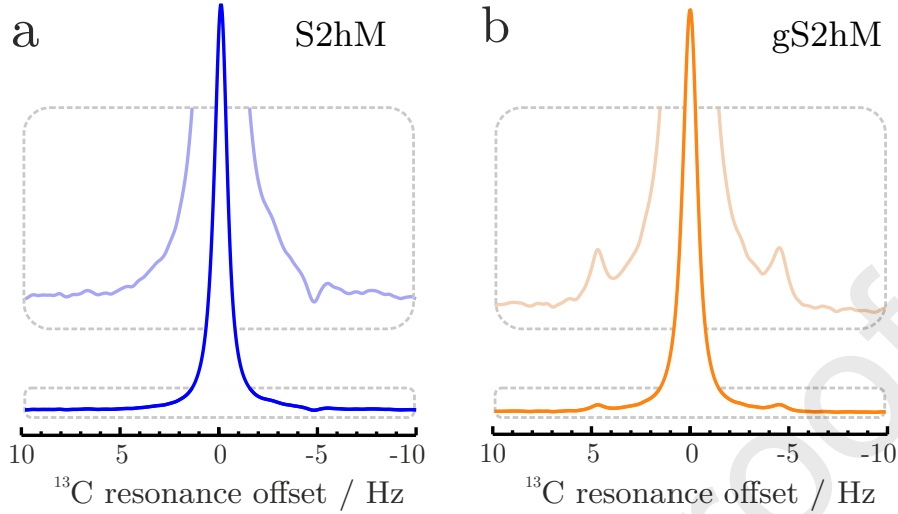


**Figure 7:** Experimental (a) M2S-S2hM and (b) M2S-gS2hM  $^{13}\text{C}$  spectra for 1- $^{13}\text{C}$  fumaric acid solution, obtained using the protocol in figure 5.  $^1\text{H}$  decoupling was not used. The pulse sequence delays and loop numbers are summarised in table 4.

**Table 5**

Theoretical and experimental pulse sequence parameters for 1- $^{13}\text{C}$ -maleic acid solution. The notation is as in table 4.

	S2hM	gS2hM
$n^* = n^{\text{exp}}$	1	3
$\tau_1^*/\text{ms}$	18.7	16.7
$\tau_1^{\text{exp}}/\text{ms}$	21.4	16.6
$\tau_2^*/\text{ms}$	18.7	10.1
$\tau_2^{\text{exp}}/\text{ms}$	21.4	7.5

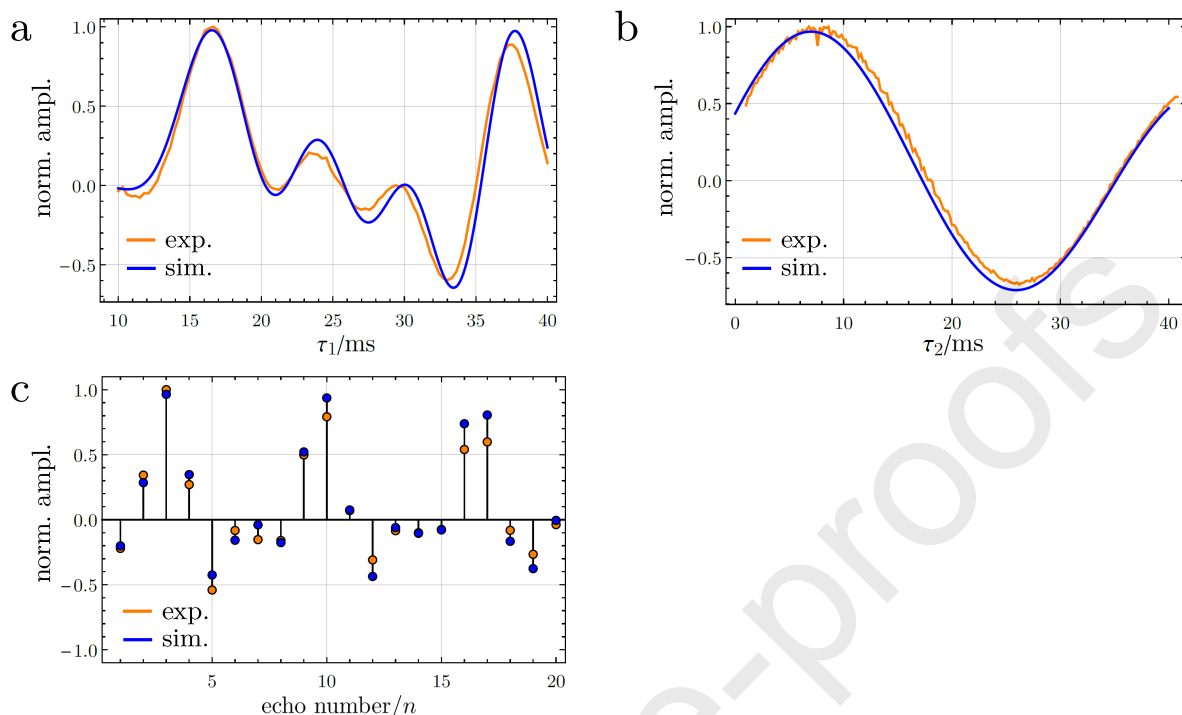
were both normalized by dividing the data by the maximum amplitude in the series. The normalised experimental data and simulations are in good qualitative agreement. Maximal  $^{13}\text{C}$  signal amplitudes were observed for echo delays  $\tau_1^{\text{exp}} = 16.6$  ms and  $\tau_2^{\text{exp}} = 7.5$  ms. Table 5 shows good agreement between empirically optimised echo delays and theoretical predictions. The experimentally optimised echo delay  $\tau_2^{\text{exp}} = 7.5$  ms is roughly 2 ms shorter than the analytic prediction  $\tau_2^* = 10.1$  ms. The experimental optimum does agree with the simulations shown in Figure 8, so we attribute the discrepancy to the approximations used in the analytical theory.

Figure 8c displays the dependence of the  $^{13}\text{C}$  signal amplitude on the echo number  $n$  for the optimised intervals  $\tau_1^{\text{exp}} = 16.6$  ms and  $\tau_2^{\text{exp}} = 7.5$  ms. In contrast to the 1- $^{13}\text{C}$ -fumaric acid solution, the echo number dependence for 1- $^{13}\text{C}$ -maleic acid solution displays an irregular behaviour. This is a direct consequence of the larger mixing angle displayed by 1- $^{13}\text{C}$ -maleate. For large mixing angles increasing or decreasing the echo number even by a single unit strongly influences the performance of the sequence, as can be seen for echo numbers  $n = 10$  and  $n = 11$ , for example.

Figure 9 shows  $^{13}\text{C}$  spectra of 1- $^{13}\text{C}$ -maleic acid solution obtained via the experimental protocol in figure 5 using either the S2hM or gS2hM sequence for the final spin order transfer step. The echo delays and echo numbers for the S2hM and gS2hM sequences are given by the experimentally optimised values in table 5. The gS2hM sequence clearly produces a more intense spectrum than the S2hM sequence for this intermediate-regime spin system. Additionally the outer peaks of the  $^{13}\text{C}$  multiplet for the gS2hM display similar intensities, whereas the outer peaks for the S2hM spectrum are slightly asymmetric. The ratio of integrated spectral amplitudes is given by  $a_{\text{gS2hM}}/a_{\text{S2hM}} = 1.20$ .

An estimate of the experimental transformation amplitudes for the two sequences was obtained by the procedure given in Appendix 2. For 1- $^{13}\text{C}$ -maleic acid solution the experimental transformation amplitudes are  $\zeta = 0.83 \pm 0.05$

## Generalised S2hM sequence



**Figure 8:** Experimental and simulated  $^{13}\text{C}$  signal amplitudes for the gS2hM sequence applied to 1- $^{13}\text{C}$ -maleic acid solution. Simulations were performed for the gS2hM transfer step assuming the coupling and pulse sequence parameters in tables 2 and 3. The experimental data sets (orange) and simulations (blue) were normalised to unity by dividing each data point by the maximum amplitude in the series. (a) Signal amplitude as a function of the echo interval  $\tau_1$  with fixed interval  $\tau_2 = 7.5$  ms and echo number  $n = 3$ . (b) Signal amplitude as a function of the free evolution delay  $\tau_2$  with fixed interval  $\tau_1 = 16.6$  ms and echo number  $n = 3$ . (c) Signal amplitude as a function of the echo number  $n$  with fixed intervals  $\tau_1 = 16.6$  ms and  $\tau_2 = 7.5$  ms.

for the gS2hM sequence and  $\zeta = 0.69 \pm 0.04$  for the S2hM sequence. Both values are in reasonable agreement with the theoretical predictions in figure 2, with the losses attributed to relaxation and experimental imperfections.

## 5. Discussion

Many experimental schemes have been proposed for the conversion of spin-pair singlet order into magnetization of a third nucleus, especially in the context of parahydrogen-enhanced NMR [44–48, 50, 51, 56, 57, 63, 76–78]. It is not our intention to thoroughly review all of these schemes here. A review and comparison of many pulse sequences, suitable for application in the high-field NMR context, was given by Bär *et al.* in 2012 [63]. A more recent review has been given by Stevanato [43]. A brief summary of the current landscape is as follows:

- The proposed pulse sequences divide into those that require resonant irradiation on both the  $I$ -spin (usually  $^1\text{H}$ ) and  $S$ -spin (often  $^{13}\text{C}$ ) channels.
- Most of the single-channel pulse sequences are very sensitive to deviations in the static magnetic field strength, or equivalently, to resonance offset effects. This undesirable feature applies, for example, to the single-channel versions of the sequences by Goldman and Jóhannesson [46], and by Kadlecik [47]. The same criticism applies to SLIC (Spin-Lock-Induced Crossing) type methods [34] in the heteronuclear context [50, 52–54], and

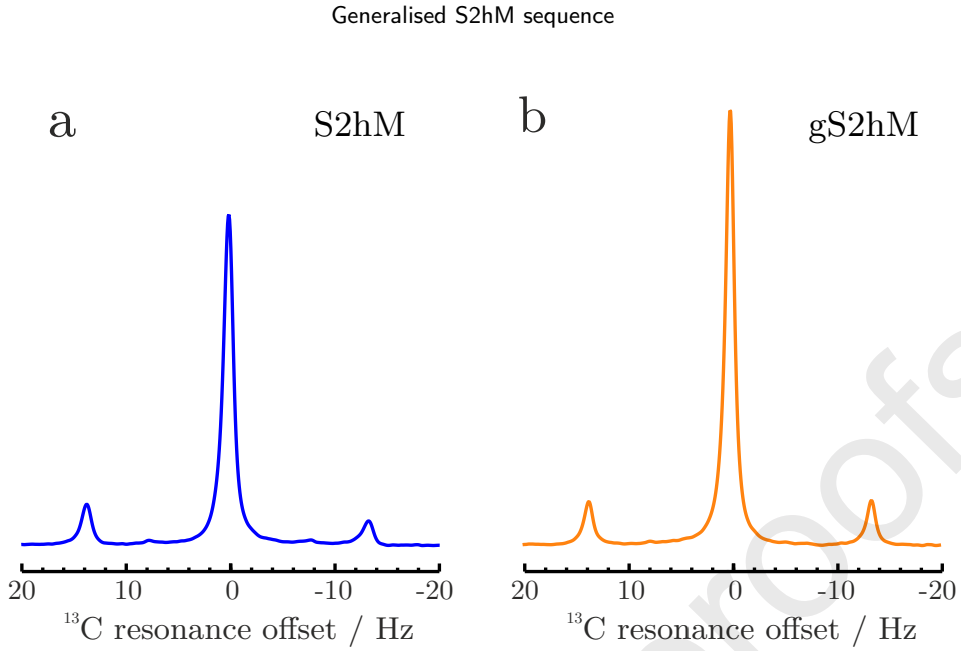


**Figure 9:** Experimental (a) M2S-S2hM and (b) M2S-gS2hM  $^{13}\text{C}$  spectra for 1- $^{13}\text{C}$  maleic acid solution, obtained using the protocol in figure 5.  $^1\text{H}$  decoupling was not used. The pulse sequence delays and loop numbers are summarised in table 5.

to the heteronuclear ADAPT (Alternating Delays Achieve Polarization Transfer) sequence [56]. The S2hM sequence [57] and the current gS2hM sequence are rare examples of single-channel pulse sequences which are insensitive to resonance offset and static field deviations.

- Many single-channel pulse sequences may be rendered insensitive to resonance offset and static field deviations by inserting  $\pi$  pulses on both the  $I$ -spin and the  $S$ -spin channels. This applies for example to the Goldman-Jóhannesson [46] and Kadlecsek [47] sequences. However, the improvement in robustness is achieved at the expense of an increase in complexity and the introduction of additional error sources.
- Schemes which involve smooth variations in the radio-frequency field strength and/or frequency, instead of discrete strong pulses, hold much promise in this area. One group of methods involves near-adiabatic transformations which may be highly robust [35, 36]. However, such methods often require individual numerical optimizations of the shape for each experimental context. Analytical solutions are not generally available.

The issue of robustness with respect to static field deviations or resonance offsets is explored in figure 10. This shows simulations of  $\zeta$  against  $S$ -spin resonance offset  $\Omega^S$  for the S2hM and gS2hM sequence, as well as the single-channel version of the Kadlecsek(2b) sequence [47]. On resonance, the Kadlecsek(2b) sequence converts singlet order into heteronuclear magnetisation with an efficiency close to the theoretical maximum. However, the heteronuclear magnetisation oscillates in sign as a function of resonance offset, while the performance of the S2hM and gS2hM sequences is almost unchanged. As mentioned above, the Kadlecsek sequence may be compensated for resonance offsets by including numerous two-channel  $\pi$  pulses [63], but this comes at the expense of increased complexity and provision of an additional rf channel.

Figure 2 illustrates the same point, but this time for the single-channel version of the sequence by Goldman and Jóhannesson [46], using pulse sequence parameters given by the analytic solutions in reference 63. The black curve in figure 2(a) shows that the Goldman-Jóhannesson sequence performs well in the intermediate coupling regime  $\theta_{\text{ST}} \simeq \pi/4$ . However, figure 2(b) shows that its performance is greatly degraded when a normal distribution of resonance offsets is included in the simulation, while the performances of the S2hM and gS2hM sequences are essentially unchanged.

The simulations in figure 2(b) include a normal distribution of resonance offsets with standard deviation  $\sigma = 2\omega_e$ , where  $\omega_e = 2\pi\{J_{12}^2 + \frac{1}{4}(J_{13} - J_{23})^2\}^{1/2}$ , in order to provide a comparable spread in offsets as the angle  $\theta_{\text{ST}}$  changes

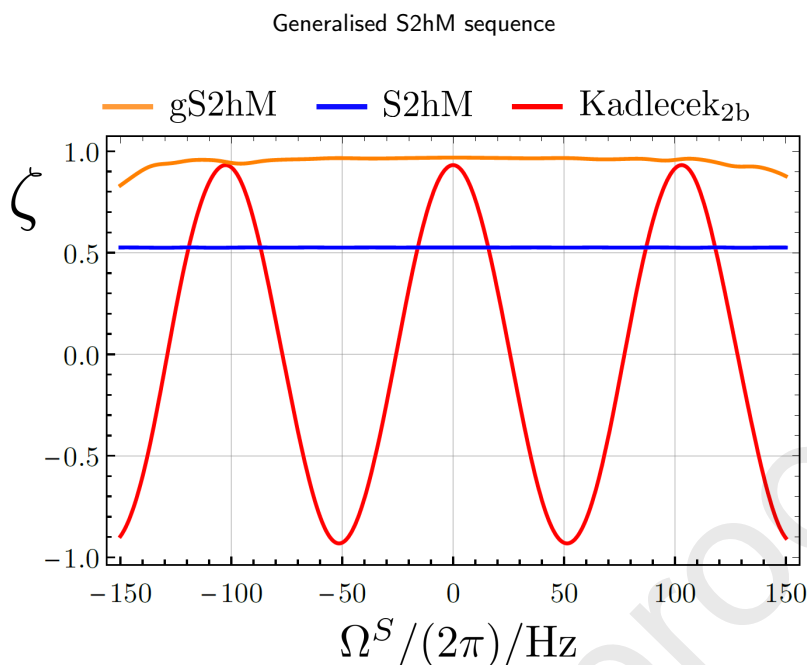


**Figure 10:** Numerical transformation amplitudes of homonuclear singlet order into heteronuclear magnetisation for a system with  $J_{12} = 12.3$  Hz,  $J_{13} = 2.1$  Hz,  $J_{23} = 13.2$  Hz and a rf field amplitude corresponding to a nutation frequency of 1 kHz. Simulated transformation amplitude curves are shown for the single-channel gS2hM (orange), S2hM (blue) and Kadlecsek(2b) (red) sequences as a function of the offset frequency  $\Omega^S$ . Simulations of the S2hM and gS2hM sequences followed the description in section 3. Simulations of the Kadlecsek(2b) sequence followed the description given in reference 47. For all sequences, individual pulses were replaced by composite pulse counterparts as described in section 3. The parameters for the S2hM and Kadlecsek(2b) sequences are derived from the analytic solutions given in reference 50 and reference 47, respectively. The pulse sequence parameters for the gS2hM sequence are derived using the analytic solutions in table 1.

across the plot. Consider for example  $1\text{-}^{13}\text{C}$ -maleic acid. Table 2 indicates that maleic acid displays a mixing angle of  $\theta_{ST} \simeq 24^\circ$  and an effective frequency of  $\omega_e/(2\pi) \simeq 13.5$  Hz. The corresponding standard deviation is given by  $\sigma/(2\pi) \simeq 27$  Hz. Conventional imaging magnets and low-field NMR setups however typically only reach static magnetic field homogeneities on the order of parts-per-million. At magnetic fields strengths ranging from 0.5 T to 3 T,  $^{13}\text{C}$  resonance offset distributions with standard deviations of several tens of Hertz are therefore not unusual and robustness against offset errors is vital. Within this regime the gS2hM sequence has significant advantages over the other strong pulse methods, while at the same time preserving a relatively low degree of complexity.

## Conflicts of interest

There are no conflicts to declare.

## Acknowledgements

This project was funded by the Marie Skłodowska-Curie program of the European Union (grant number 766402), the European Research Council (786707-FunMagResBeacons), and EPSRC-UK (grants EP/P009980/1 and EP/P030491/1).

## Generalised S2hM sequence

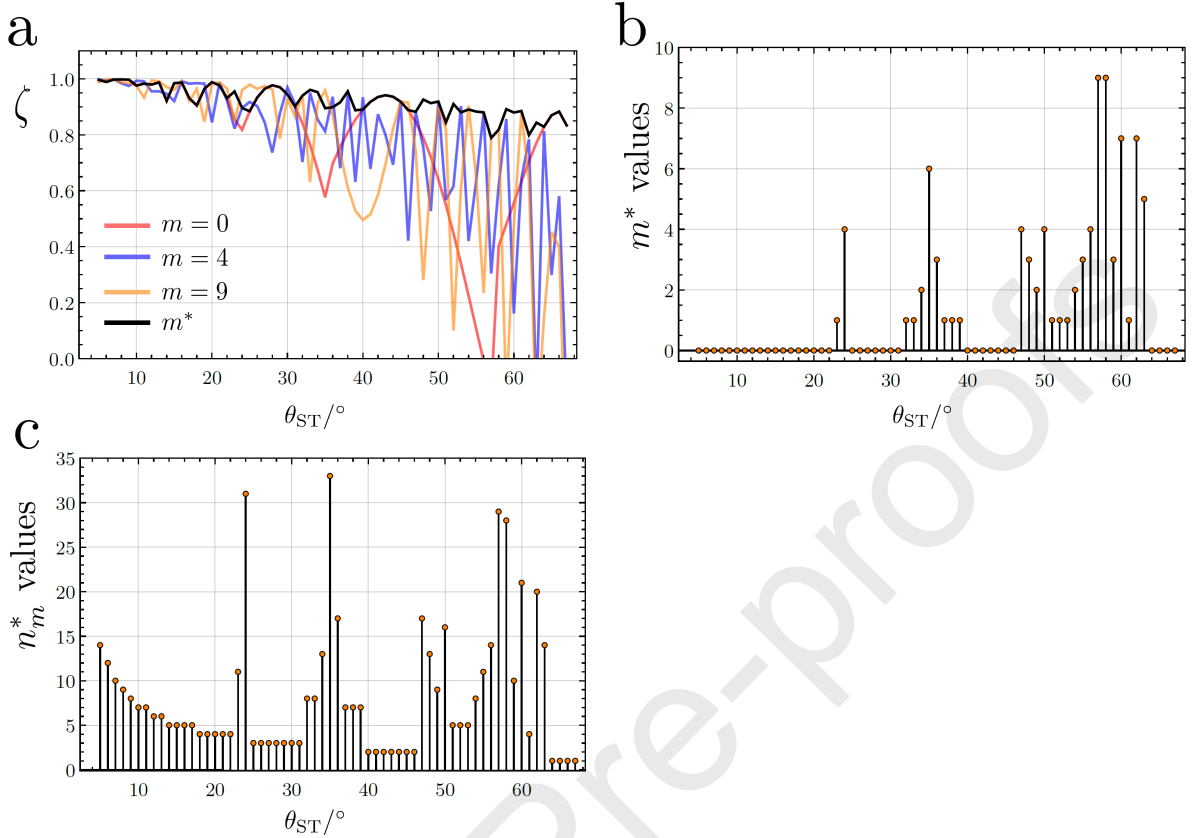


**Figure 11:** (a) gS2hM transformation amplitudes for conversion of singlet order into heteronuclear Zeeman order as a function of the mixing angle  $\theta_{ST}$  for echo number families  $n_m^*$  with  $m \in \{0, 4, 9\}$ . For each value of  $\theta_{ST}$ , the maximum transformation amplitude provided by the cases  $m \in \{0, \dots, 9\}$  is shown in black and denoted by  $m^*$ . (b) Overview of the values of  $m^*$  leading to the black trajectory in figure (a). (c) Resulting overall echo numbers  $n_m^* = \text{round}((2m^* + 1)\pi/\xi^*)$  for the selected values of  $m^*$  shown in figure (b).

## Appendices

### Appendix 1. Optimal echo numbers

As discussed in section 2.4, the gS2hM sequence displays dips in performance for certain mixing angles  $\theta_{ST}$ . These dips occur whenever the effective rotation angle  $\xi$  lies approximately halfway between two whole numbers,

$$\pi/\xi^* \simeq p + \frac{1}{2} \quad (64)$$

where  $p$  is an integer. For such cases, the "round" instruction in table 1 does not represent a good compromise.

Instead it is possible to make use of the periodicity of the spin dynamics to define a family of approximate echo numbers

$$n_m^* = \text{round}((2m + 1)\pi/\xi^*) \quad \text{with} \quad m \in \{0, 1, 2, \dots\}, \quad (65)$$

characterised by the integer  $m$ . The integer  $m$  provides some additional flexibility and may be used to increase the performance of the gS2hM sequence. Figure 11(a) illustrates the performance of the gS2hM sequence for different echo number families  $n_m^*$  as a function of the mixing angle  $\theta_{ST}$ . Simulations have been performed for values of  $m$  ranging from 0 to 9. The evolution delays  $\tau_1$  and  $\tau_2$  of the gS2hM sequence have been determined according to the

analytic solutions summarised in table 1. For the sake of clarity, figure 11(a) only highlights transformation amplitudes for  $m \in \{0, 4, 9\}$  given by the transparent curves.

As can be seen neither of the  $m$  values on their own provide a flat transformation amplitude profile for the full range of mixing angles. Instead individual families follow a saw-tooth pattern with occasional dips. For example, a large dip may be seen at  $\theta_{ST} \simeq 57^\circ$  for the  $m = 0$  family shown in red. As pointed out above, dips of this type occur whenever the ratio  $\pi/\xi^*$  lies close to the halfway point between two integers.

The black line in figure 11(a) shows a compilation of the best transformation amplitudes achieved within the considered set  $m \in \{0, \dots, 9\}$ . As can be seen, the additional flexibility provided by the optional integer  $m$  stabilises the performance of the gS2hM sequence, and the transformation amplitudes remain above 85% for all mixing angles  $0 < \theta_{ST} < 67.5^\circ$ . However, one drawback of this procedure is that a numerical search is required to find the optimal number  $m$  for a given mixing angle  $\theta_{ST}$ .

For practical applications there is a clear payoff between a small echo number  $n^*$ , accurate theoretical performance, and a long pulse sequence duration leading to relaxation losses. The total echo numbers corresponding to the optimal theoretical amplitudes are indicated in figure 11(b). For the most part the echo numbers stay well below  $n^* = 15$ . A selected few regions require echo numbers above  $n > 20$ . These may still be generated by making use of equation 65, albeit with larger values of  $m$ .

## Appendix 2. Experimental estimation of transformation amplitudes

To isolate the S2hM and gS2hM transformation amplitudes we follow the line of reasoning presented in reference 50. For simplicity we make the following abbreviations

$$A = \frac{1}{4}(I_{1z} + I_{2z}), \quad B = \frac{1}{2}SO, \quad C = \frac{1}{4}I_{3z}. \quad (66)$$

The amplitude  $a_I$  of a single pulse acquire spectrum on the  $I$  spin channel is directly proportional to the  $I$  spin equilibrium magnetisation

$$a_I = f_I p_{eq}^I \quad (67)$$

with  $f_I$  being an instrumental constant for detection on the  $I$  spin channel. The signal amplitude for a M2S-gS2M experiment may then be expressed as follows

$$a_1 = f_I p_{eq}^I \langle A \xrightarrow{\text{M2S}} B \rangle \langle B \xrightarrow{\text{gS2M}} A \rangle = a_I \langle A \xrightarrow{\text{M2S}} B \rangle \langle B \xrightarrow{\text{gS2M}} A \rangle. \quad (68)$$

The transformation amplitudes for M2S and gS2M are related as shown below [50]

$$\zeta_{\text{M2S}}^{\text{exp}} = \langle B \xrightarrow{\text{gS2M}} A \rangle = \frac{3}{2} \langle A \xrightarrow{\text{M2S}} B \rangle \quad (69)$$

and may be used to express  $a_{\text{M2S}}$  in a more concise way

$$a_1 = \frac{3}{2} a_I \langle A \xrightarrow{\text{M2S}} B \rangle^2. \quad (70)$$

The transformation amplitude for a single M2S step is then given by

$$\langle A \xrightarrow{\text{M2S}} B \rangle = \pm \sqrt{\frac{2}{3} \frac{a_1}{a_I}}. \quad (71)$$

Similarly the amplitude  $a_S$  of a single pulse acquire spectrum on the  $S$  spin channel is given by

$$a_S = f_S p_{eq}^S, \quad (72)$$

with  $f_S$  being an instrumental constant for detection on the  $S$  spin channel. The transformation amplitude for the M2S-gS2hM (M2S-gS2hM) block is decomposed as follows

$$a_2 = f_S p_{eq}^I \langle A \xrightarrow{\text{M2S}} B \rangle \langle B \xrightarrow{\text{gS2hM}} C \rangle = \pm f_S p_{eq}^S \frac{\gamma_I}{\gamma_S} \sqrt{\frac{2}{3} \frac{a_1}{a_I}} \langle B \xrightarrow{\text{gS2hM}} C \rangle \approx 4a_S \sqrt{\frac{2}{3} \frac{a_1}{a_I}} \langle B \xrightarrow{\text{gS2hM}} C \rangle. \quad (73)$$

## Generalised S2hM sequence

**Table 6**

Estimates of experimental transformation amplitudes for the M2S, S2hM and gS2hM sequences.

1- <sup>13</sup> C fumaric acid			1- <sup>13</sup> C maleate		
M2S	gS2hM	S2hM	M2S	gS2hM	S2hM
$a_1/a_I$	$a_2/a_S$	$a_2/a_S$	$a_1/a_I$	$a_2/a_S$	$a_2/a_S$
0.31	1.48	1.60	0.33	1.55	1.30
$\zeta_{\text{M2S}}^{\text{exp}}$	$\zeta_{\text{gS2hM}}^{\text{exp}}$	$\zeta_{\text{S2hM}}^{\text{exp}}$	$\zeta_{\text{M2S}}^{\text{exp}}$	$\zeta_{\text{gS2hM}}^{\text{exp}}$	$\zeta_{\text{S2hM}}^{\text{exp}}$
0.49	0.81	0.88	0.49	0.82	0.69

The transformation amplitude  $\langle B \xrightarrow{\text{gS2hM}} C \rangle$  for  $I$  spin singlet order to  $S$  spin Zeeman order step may then be extracted as shown below

$$\zeta_{\text{gS2hM}}^{\text{exp}} = \langle B \xrightarrow{\text{gS2hM}} C \rangle = \pm \frac{a_2}{4a_S} \sqrt{\frac{3}{2} \frac{a_I}{a_1}}. \quad (74)$$

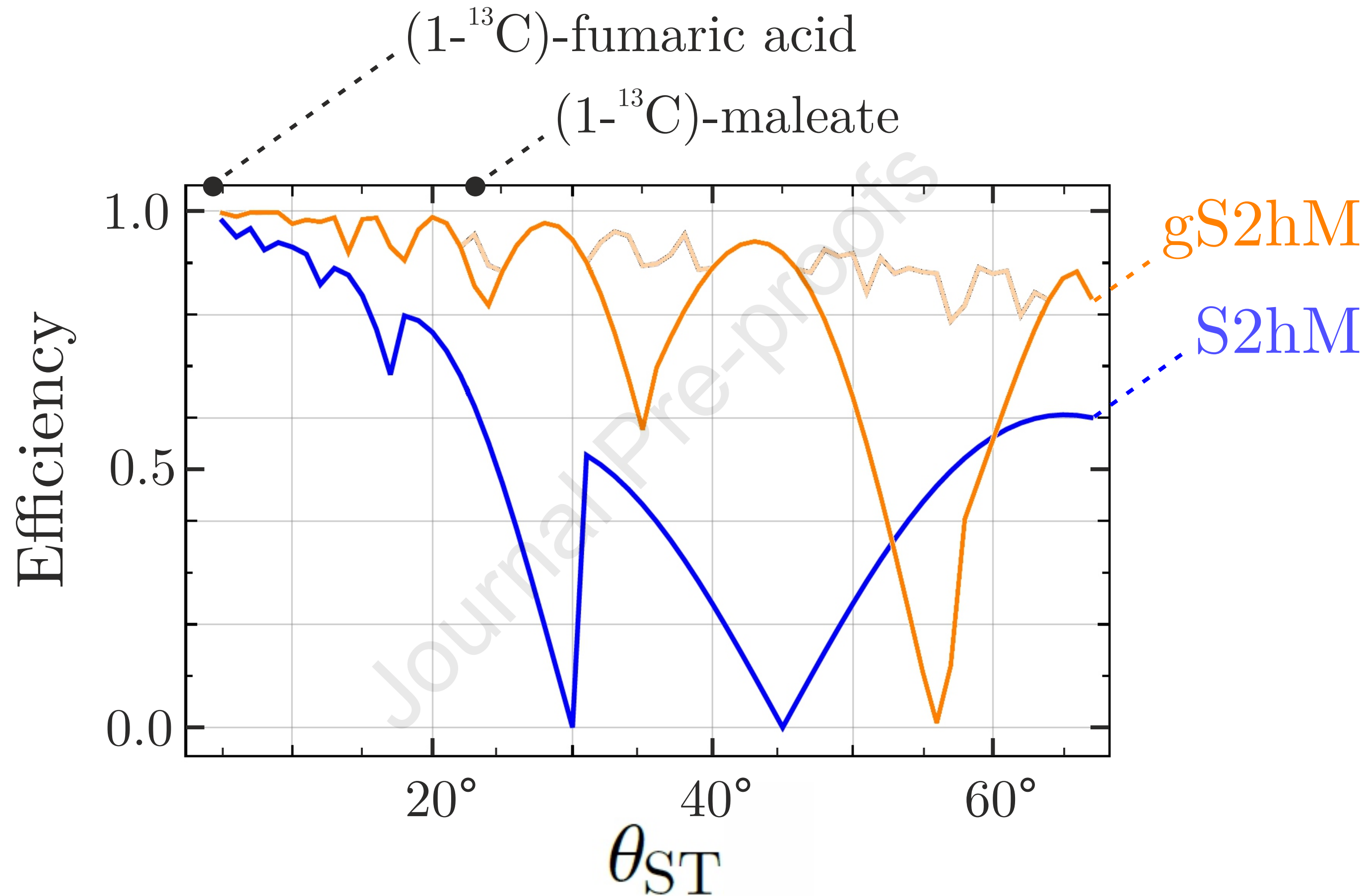
Experimentally obtained transformation amplitudes for the instrumental setup discussed in section 3 are summarised in table 6.

## References

- [1] R. Sarkar, P. Ahuja, P. R. Vasos and G. Bodenhausen, *Physical Review Letters*, 2010, **104**, 053001.
- [2] S. Cavadini and P. R. Vasos, *Concepts in Magnetic Resonance Part A*, 2008, **32A**, 68–78.
- [3] P. Ahuja, R. Sarkar, P. R. Vasos and G. Bodenhausen, *Journal of the American Chemical Society*, 2009, **131**, 7498–7499.
- [4] N. Salvi, R. Buratto, A. Bornet, S. Ulzega, I. Rentero Rebollo, A. Angelini, C. Heinis and G. Bodenhausen, *Journal of the American Chemical Society*, 2012, **134**, 11076–11079.
- [5] G. Pileio and S. Ostrowska, *Journal of Magnetic Resonance (San Diego, Calif.: 1997)*, 2017, **285**, 1–7.
- [6] J. Eills, W. Hale, M. Sharma, M. Rossetto, M. H. Levitt and M. Utz, *Journal of the American Chemical Society*, 2019, **141**, 9955–9963.
- [7] M. Carravetta, O. G. Johannessen and M. H. Levitt, *Physical Review Letters*, 2004, **92**, 153003.
- [8] G. Stevanato, S. S. Roy, J. Hill-Cousins, I. Kuprov, L. J. Brown, R. C. D. Brown, G. Pileio and M. H. Levitt, *Physical Chemistry Chemical Physics*, 2015, **17**, 5913–5922.
- [9] *Long-lived Nuclear Spin Order: Theory and Applications*, ed. G. Pileio, Royal Society of Chemistry, S.I., 1st edn., 2020.
- [10] C. R. Bowers and D. P. Weitekamp, *Physical Review Letters*, 1986, **57**, 2645–2648.
- [11] C. R. Bowers and D. P. Weitekamp, *Journal of the American Chemical Society*, 1987, **109**, 5541–5542.
- [12] L. R. Becerra, G. J. Gerfen, R. J. Temkin, D. J. Singel and R. G. Griffin, *Physical Review Letters*, 1993, **71**, 3561–3564.
- [13] J. H. Ardenkjaer-Larsen, B. Fridlund, A. Gram, G. Hansson, L. Hansson, M. H. Lerche, R. Servin, M. Thaning and K. Golman, *Proceedings of the National Academy of Sciences of the United States of America*, 2003, **100**, 10158–10163.
- [14] A. M. Balu, S. B. Duckett and R. Luque, *Dalton Transactions*, 2009, 5074–5076.
- [15] C. Griesinger, M. Bennati, H. M. Vieth, C. Luchinat, G. Parigi, P. Höfer, F. Engelke, S. J. Glaser, V. Denysenkov and T. F. Prisner, *Progress in Nuclear Magnetic Resonance Spectroscopy*, 2012, **64**, 4–28.
- [16] M. C. D. Tayler, I. Marco-Rius, M. I. Kettunen, K. M. Brindle, M. H. Levitt and G. Pileio, *Journal of the American Chemical Society*, 2012, **134**, 7668–7671.
- [17] B. Meier, J.-N. Dumez, G. Stevanato, J. T. Hill-Cousins, S. S. Roy, P. Håkansson, S. Mamone, R. C. D. Brown, G. Pileio and M. H. Levitt, *Journal of the American Chemical Society*, 2013, **135**, 18746–18749.
- [18] G. Pileio, S. Bowen, C. Laustsen, M. C. D. Tayler, J. T. Hill-Cousins, L. J. Brown, R. C. D. Brown, J. H. Ardenkjaer-Larsen and M. H. Levitt, *Recycling and Imaging of Nuclear Singlet Hyperpolarization*, 2013, <https://pubs.acs.org/doi/abs/10.1021/ja312333v>.
- [19] I. Marco-Rius, M. C. D. Tayler, M. I. Kettunen, T. J. Larkin, K. N. Timm, E. M. Serrao, T. B. Rodrigues, G. Pileio, J. H. Ardenkjaer-Larsen, M. H. Levitt and K. M. Brindle, *NMR in Biomedicine*, 2013, **26**, 1696–1704.
- [20] A. Bornet, X. Ji, D. Mammoli, B. Vuichoud, J. Milani, G. Bodenhausen and S. Jannin, *Chemistry – A European Journal*, 2014, **20**, 17113–17118.
- [21] B. Vuichoud, J. Milani, A. Bornet, R. Melzi, S. Jannin and G. Bodenhausen, *The Journal of Physical Chemistry B*, 2014, **118**, 1411–1415.
- [22] A. S. Kiryutin, H. Zimmermann, A. V. Yurkovskaya, H.-M. Vieth and K. L. Ivanov, *Journal of Magnetic Resonance*, 2015, **261**, 64–72.
- [23] A. Jhajharia, E. M. M. Weber, J. G. Kempf, D. Abergel, G. Bodenhausen and D. Kurzbach, *The Journal of Chemical Physics*, 2017, **146**, 041101.
- [24] S. S. Roy, K. M. Appleby, E. J. Fear and S. B. Duckett, *The Journal of Physical Chemistry Letters*, 2018, **9**, 1112–1117.
- [25] B. Proccacci, S. S. Roy, P. Norcott, N. Turner and S. B. Duckett, *Journal of the American Chemical Society*, 2018, **140**, 16855–16864.
- [26] W. Iali, S. S. Roy, B. J. Tickner, F. Ahwal, A. J. Kennerley and S. B. Duckett, *Angewandte Chemie*, 2019, **131**, 10377–10381.
- [27] M. H. Levitt, *Journal of Magnetic Resonance*, 2019, **306**, 69–74.
- [28] M. H. Levitt, in *Long-lived Nuclear Spin Order: Theory and Applications*, Royal Society of Chemistry, 1st edn., 2020, p. 300.
- [29] C. Bengs, *The Journal of Chemical Physics*, 2020, **152**, 054106.
- [30] R. Sarkar, P. Ahuja, D. Moskau, P. R. Vasos and G. Bodenhausen, *ChemPhysChem*, 2007, **8**, 2652–2656.
- [31] G. Pileio, M. Carravetta, E. Hughes and M. H. Levitt, *Journal of the American Chemical Society*, 2008, **130**, 12582–12583.
- [32] G. Pileio, M. Carravetta and M. H. Levitt, *Proceedings of the National Academy of Sciences*, 2010, **107**, 17135–17139.
- [33] M. C. D. Tayler and M. H. Levitt, *Physical Chemistry Chemical Physics*, 2011, **13**, 5556–5560.
- [34] S. J. DeVience, R. L. Walsworth and M. S. Rosen, *Physical Review Letters*, 2013, **111**, 173002.
- [35] A. N. Pravdivtsev, A. S. Kiryutin, A. V. Yurkovskaya, H.-M. Vieth and K. L. Ivanov, *Journal of Magnetic Resonance*, 2016, **273**, 56–64.
- [36] B. A. Rodin, K. F. Sheberstov, A. S. Kiryutin, J. T. Hill-Cousins, L. J. Brown, R. C. D. Brown, B. Jamain, H. Zimmermann, R. Z. Sagdeev, A. V. Yurkovskaya and K. L. Ivanov, *The Journal of Chemical Physics*, 2019, **150**, 064201.
- [37] S. J. Elliott and G. Stevanato, *Journal of Magnetic Resonance*, 2019, **301**, 49–55.
- [38] B. Kharkov, X. Duan, E. S. Tovar, J. W. Canary and A. Jerschow, *Physical Chemistry Chemical Physics*, 2019, **21**, 2595–2600.
- [39] S. Mamone, N. Rezaei-Ghaleh, F. Opazo, C. Griesinger and S. Glöggler, *Science Advances*, 2020, **6**, eaaz1955.
- [40] C. Bengs, M. Sabba, A. Jerschow and M. H. Levitt, *Physical Chemistry Chemical Physics*, 2020, **22**, 9703–9712.
- [41] R. R. Ernst, G. Bodenhausen and A. Wokaun, *Principles of Nuclear Magnetic Resonance in One and Two Dimensions*, Clarendon Press, 1990, vol. 1.
- [42] M. H. Levitt, *Spin dynamics: basics of nuclear magnetic resonance*, Wiley, 2001.
- [43] G. Stevanato, in *Long-lived Nuclear Spin Order*, Royal Society of Chemistry, 2020, pp. 209–225.
- [44] M. Haake, J. Natterer and J. Bargon, *Journal of the American Chemical Society*, 1996, **118**, 8688–8691.
- [45] J. Barkemeyer, J. Bargon, H. Sengtschmid and R. Freeman, *Journal of Magnetic Resonance, Series A*, 1996, **120**, 129–132.
- [46] M. Goldman and H. Jóhannesson, *Comptes Rendus Physique*, 2005, **6**, 575–581.
- [47] S. Kadlecěk, K. Emami, M. Ishii and R. Rizi, *Journal of Magnetic Resonance*, 2010, **205**, 9–13.
- [48] C. Cai, A. M. Coffey, R. V. Shchepin, E. Y. Chekmenev and K. W. Waddell, *The Journal of Physical Chemistry B*, 2013, **117**, 1219–1224.
- [49] A. N. Pravdivtsev, A. V. Yurkovskaya, N. N. Lukzen, K. L. Ivanov and H.-M. Vieth, *The Journal of Physical Chemistry Letters*, 2014, **5**, 3421–3426.

## Generalised S2hM sequence

- [50] J. Eills, G. Stevanato, C. Bengs, S. Glöggler, S. J. Elliott, J. Alonso-Valdesueiro, G. Pileio and M. H. Levitt, *Journal of Magnetic Resonance*, 2017, **274**, 163–172.
- [51] S. Korchak, S. Yang, S. Mamone and S. Glöggler, *ChemistryOpen*, 2018, **7**, 344–348.
- [52] T. Theis, M. Truong, A. M. Coffey, E. Y. Chekmenev and W. S. Warren, *Journal of Magnetic Resonance (San Diego, Calif.: 1997)*, 2014, **248**, 23–26.
- [53] A. N. Pravdivtsev, A. V. Yurkovskaya, H.-M. Vieth and K. L. Ivanov, *The Journal of Physical Chemistry B*, 2015, **119**, 13619–13629.
- [54] S. Knecht, A. S. Kiryutin, A. V. Yurkovskaya and K. L. Ivanov, *Molecular Physics*, 2019, **117**, 2762–2771.
- [55] A. N. Pravdivtsev, A. V. Yurkovskaya, H. Zimmermann, H.-M. Vieth and K. L. Ivanov, *RSC Advances*, 2015, **5**, 63615–63623.
- [56] G. Stevanato, *Journal of Magnetic Resonance*, 2017, **274**, 148–162.
- [57] G. Stevanato, J. Eills, C. Bengs and G. Pileio, *Journal of Magnetic Resonance*, 2017, **277**, 169–178.
- [58] S. Appelt, F. W. Häsing, H. Kühn, U. Sieling and B. Blümich, *Chemical Physics Letters*, 2007, **440**, 308–312.
- [59] S. Appelt, F. W. Häsing, U. Sieling, A. Gordji-Nejad, S. Glöggler and B. Blümich, *Physical Review A*, 2010, **81**, 023420.
- [60] T. Theis, J. W. Blanchard, M. C. Butler, M. P. Ledbetter, D. Budker and A. Pines, *Chemical Physics Letters*, 2013, **580**, 160–165.
- [61] M. C. Butler, M. P. Ledbetter, T. Theis, J. W. Blanchard, D. Budker and A. Pines, *The Journal of Chemical Physics*, 2013, **138**, 184202.
- [62] J. W. Blanchard and D. Budker, in *eMagRes*, American Cancer Society, 2016, pp. 1395–1410.
- [63] S. Bär, T. Lange, D. Leibfritz, J. Hennig, D. v. Elverfeldt and J.-B. Hövener, *Journal of Magnetic Resonance*, 2012, **225**, 25–35.
- [64] C. Bengs and M. H. Levitt, *Magnetic Resonance in Chemistry*, 2018, **56**, 374–414.
- [65] O. W. Sørensen, *Journal of Magnetic Resonance (1969)*, 1990, **86**, 435 – 440.
- [66] M. H. Levitt, *Journal of Magnetic Resonance*, 2016, **262**, 91–99.
- [67] S. Vega and A. Pines, *The Journal of Chemical Physics*, 1977, **66**, 5624–5644.
- [68] S. Vega, *The Journal of Chemical Physics*, 1978, **68**, 5518–5527.
- [69] A. Wokaun and R. R. Ernst, *The Journal of Chemical Physics*, 1977, **67**, 1752–1758.
- [70] M. J. Frisch, G. W. Trucks, H. B. Schlegel, G. E. Scuseria, M. A. Robb, J. R. Cheeseman, G. Scalmani, V. Barone, G. A. Petersson, H. Nakatsuji, X. Li, M. Caricato, A. V. Marenich, J. Bloino, B. G. Janesko, R. Gomperts, B. Mennucci, H. P. Hratchian, J. V. Ortiz, A. F. Izmaylov, J. L. Sonnenberg, Williams, F. Ding, F. Lipparini, F. Egidi, J. Goings, B. Peng, A. Petrone, T. Henderson, D. Ranasinghe, V. G. Zakrzewski, J. Gao, N. Rega, G. Zheng, W. Liang, M. Hada, M. Ehara, K. Toyota, R. Fukuda, J. Hasegawa, M. Ishida, T. Nakajima, Y. Honda, O. Kitao, H. Nakai, T. Vreven, K. Throssell, J. A. Montgomery Jr., J. E. Peralta, F. Ogliaro, M. J. Bearpark, J. J. Heyd, E. N. Brothers, K. N. Kudin, V. N. Staroverov, T. A. Keith, R. Kobayashi, J. Normand, K. Raghavachari, A. P. Rendell, J. C. Burant, S. S. Iyengar, J. Tomasi, M. Cossi, J. M. Millam, M. Klene, C. Adamo, R. Cammi, J. W. Ochterski, R. L. Martin, K. Morokuma, O. Farkas, J. B. Foresman and D. J. Fox, *Gaussian 16 Rev. C.01*, 2016.
- [71] M. C. D. Tayler and M. H. Levitt, *Journal of the American Chemical Society*, 2013, **135**, 2120–2123.
- [72] M. C. D. Tayler, in *Long-lived Nuclear Spin Order*, Royal Society of Chemistry, 2020, pp. 188–208.
- [73] M. H. Levitt and R. Freeman, *Journal of Magnetic Resonance (1969)*, 1981, **43**, 502–507.
- [74] S. Wimperis, *Journal of Magnetic Resonance, Series A*, 1994, **109**, 221–231.
- [75] U. Haeberlen, *Advances in Magnetic Resonance: High Resolution N.M.R. in Solids Selective Averaging Suppt. 1*, Academic Press Inc, New York, 1976.
- [76] A. S. Kiryutin, A. V. Yurkovskaya, N. N. Lukzen, H.-M. Vieth and K. L. Ivanov, *The Journal of Chemical Physics*, 2015, **143**, 234203.
- [77] C. Laustsen, S. Bowen, M. S. Vinding, N. C. Nielsen and J. H. Ardenkjaer-Larsen, *Magnetic Resonance in Medicine*, 2014, **71**, 921–926.
- [78] J. Eills, J. W. Blanchard, T. Wu, C. Bengs, J. Hollenbach, D. Budker and M. H. Levitt, *The Journal of Chemical Physics*, 2019, **150**, 174202.



## Highlights

- Transformation of singlet order into heteronuclear magnetisation by the gS2hM sequence.
- The gS2hM sequence works in the near-equivalence regime up to the intermediate regime.
- The gS2hM sequence is insensitive to deviations in the static magnetic field and radiofrequency field strength.

**Declaration of interests**

☒ The authors declare that they have no known competing financial interests or personal relationships that could have appeared to influence the work reported in this paper.

☐ The authors declare the following financial interests/personal relationships which may be considered as potential competing interests:

--